Modeling of oil reservoirs with focus on microbial induced effects

Master's thesis in Applied and Computational Mathematics

Stanley Owulabi Babatunde

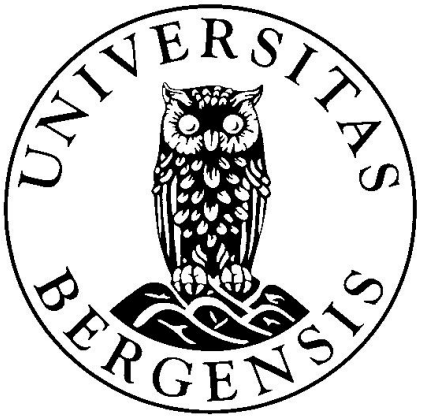

Department of Mathematics
University of Bergen

November 2014

Dedication

This piece of work is dedicated to the entire Babatunde family in Ghana, Australia and Norway for their numerous support in bringing me up this far.

Acknowledgement

All thanks and praise go to the almighty God for the courage and determination granted me to be able to put this piece together. It is solely by His grace, wisdom and knowledge which has guided me in conducting this research studies in spite of all difficulties. I am eternally grateful to Him.

My thanks also goes to my supervisors; Associate professor Florin Adrian Radu and Professor Jan Martin Nordbotten whose wonderful comments and advice have made this work a success. As a matter of fact, you made me believe that I have so much strength and courage to persevere in the midst of staggering oppositions. What kept my head up the sea was your great motivation. You understood me and were very tolerant and determined to see me through and you indeed achieved your aim. Honestly, I aspire to emulate you if I ever have the chance to step into your shoes in the future. The exposures you both gave me to attend NUPUS workshop and conference in Germany gave me much insight into research. I will never forget those memories. To all the wonderful people at the University of Stuttgart, I thank you for your kindness.

I cannot rule out the contributions of the various bibliographies and scientific papers which fed me in putting this piece together. To the various authors, I express my profound gratitude to you all.

I want to specially thank Mr. Emmanuel Babatunde and Veronica Babatunde for the immense financial support they offered me which has given me the sound mind to undertake this research work. I thank all others who assisted, encouraged and supported me during this research, not forgetting my colleague master students and my brother Kingsley Bawfeh for their support.

Last but not least, I appreciate my best friend Elorm Agoba for her words of encouragement.

It is my wish that the good Lord bless you all for the contributions you made.

Abstract

As an abstract to this thesis, we review some literatures in EOR and discussed the processes, strength and weakness of Microbial Enhanced Oil Recovery techniques. A two phase flow model comprising water and oil via the concept of mean pressure has been formulated using mass conservation equations, Darcy's law and constitutive relations. This resulted in a set of coupled nonlinear parabolic partial differential equation with primary variables being the mean pressure and water saturation. We discretized these equations in one dimension using a control volume discretization scheme in space and implicit Euler in time. We employed the IMPES approach which decoupled the primary variables. A model validation test was made by comparison with an analytical solution and with the Couplex-Gas benchmark. The model was used to investigate two major mechanisms by which the activities of bacterial helps in enhancing the recovery of the residual oil.

Contents

List of Figures

List of Tables

Abbreviations

EOR	**E**nhanced **O**il **R**ecovery
MEOR	**M**icrobial **E**nhanced **O**il **R**ecovery
REV	**R**epresentative **E**lementary **V**olume

Symbols

ϕ	Porosity of the porous medium	m
$\hat{K}$	permeability of the porous medium	MilliDarc $[mD]$
$\overrightarrow{U}$	Darcy's velocity	$[m/s]$
K_{ro}	relative permeability of oil	MilliDarc $[mD]$
K_{rw}	relative permeability of water	MilliDarc $[mD]$
$\hat{K}_o$	effective permeability of oil	MilliDarc $[mD]$
$\hat{K}_w$	effective permeability of water	MilliDarc $[mD]$
g	acceleration due to gravity	$[m/s^2]$
o	oil	
w	water	
t	time coordinate	seconds (s)
x	space coordinate	meters (m)
τ	time step	seconds (s)
h	spatial step	meters (m)
S	saturation	
S_o	saturation of oil	
S_w	saturation of water	
$\overline{P}$	mean pressure	pascal $[MPa]$
P_e	entry pressure	pascal $[MPa]$
P_c	capillary pressure	pascal $[MPa]$
P_o	pressure of oil	pascal $[MPa]$
P_w	pressure of water	pascal $[MPa]$
ρ_o	density of oil	$[kg/m^3]$

ρ_w	density of water	$[kg/m^3]$
μ_o	viscosity of oil	$[kgm^{-1}s^{-1}]$
μ_w	viscosity of water	$[kgm^{-}1s^{-}1]$
F_v^o	source/sink term of oil	
F_v^w	source/sink term of water	
F_v^T	source/sink term	
λ_T	Total mobility of the displacing fluid	
λ_d	Total mobility of the displaced fluid	
C	bacterial concentration	
D	dispersion coefficient	
ν	velocity of bacterial in water	$[m/s]$
λ	Brooks-Corey parameter for the porous medium	

Chapter 1

General introduction

Energy is an essential force which the world cannot survive without. Despite the huge investments in other sources of energy such as biofuels, solar energy and wind energy; fossil fuels will still remain the key supply of energy source for many years to come (Graus et al. 2011). The current concern the global oil industry faces is the increase rate of unproductive and ageing wells. An oil well can be said to be unproductive when approximately about 30 % of the oil in place has been recovered; thus, a substantial quantity of oil is left in them after the application of conventional oil extraction methods. Moreover, there is a dire need to produce more crude oil to meet the worldwide rising energy demand which illustrates the necessity of progressing Enhanced Oil Recovery (EOR) processes. These methods try to overcome the main obstacles in the way of efficient oil recovery such as the low permeability of some reservoirs, the high viscosity of the crude oil, and high oil-water inter-facial tensions that may result in high capillary forces retaining the excess oil in the reservoir rock (Bubela, 1987). With the global campaign on protecting the environment through reducing the green house effect by probably Carbon Capture and Storage (CCS) [11] and other possible means, a big challenge is thrown to the oil industry to come out with efficient but environmentally friendly EOR techniques.

During oil production, primary oil recovery can account for between 30-40 % oil productions, while additional 15-25 % can be recovered by secondary methods such as water injection, leaving behind about 35-55 % of oil as residual oil in the reservoirs (Cosse, 1993). This residual oil is usually the target of many enhanced

oil recovery technologies. Recovery of this residual oil is at present a big challenge for many oil companies and there is a continuous search for a cheap and efficient technology that can help in its recovery. Additional recovery from residual oil can lead to increase in global oil production as well as prolonging the productive life of many oilfields. The techniques employed for recovery of this residual oil are generally termed Enhanced Oil Recovery (EOR) methods.

Thesis outline

In chapter 2 of this work, we shall review some relevant literatures available on MEOR so as to be abreast with current trends and development in this field. A formulation of a mathematical model consisting of a two-phase flow of oil and water will be given in chapter 3. All mathematical equations encountered in this work will be discretized in one dimension using the finite volume discretization scheme and this will be organized in chapter 4. For our model to be trusted and dependable for further simulations, we will seek to either construct an analytical solution and perform some convergence analysis or run some simulations of a know benchmark to see if the results using our model will be consistent with that of the benchmark. This will be done in chapter 5. The major goal of this thesis is to analyze numerically how the introduction of bacteria into the reservoir can help to recover the residual oil. In the last two chapters 6 and 7 of this work, we shall investigate some mechanisms by which microbial models are incorporated into the reservoir for the enhancement of the residual oil. Conclusions and outlook will be given in the last chapter 7.

Chapter 2

Microbial Enhanced Oil Recovery

The notion of using Microbial Enhance Oil Recovery (MEOR) stems as far back in the 1920s where ZoBell [3] studied and observed a gradual separation of oil caused by sulfate-reducing bacteria. Ever since, there has been numerous research carried in this area which has been reported in the literature. This has been summarized by Bryant and Burchfield [4].

2.1 Phases of oil recovery

Enhanced Oil Recovery (EOR) is generally considered as the third, or last, phase of useful oil production. It is mostly referred to as the tertiary oil production. The first or primary phase of oil production begins with the discovery of an oil field using the natural stored energy to move the oil wells by expansion of volatile components or pumping of individual wells to assist the natural drive. When this oil is depleted, production declines.

A secondary phase of oil production begins when supplemental energy is added to the reservoir by injection of water. As the oil-to-water production ration of the field approaches an economic limit of operation, the net profit diminishes because the difference between the value of the produced oil and the cost of the water treatment and injection becomes too narrow, the tertiary period of production begins where the water injection phenomenon in the secondary stage is changed.

The residual oil is retained mainly by viscous and capillary forces. These forces are influenced by several parameters such as; surface/inter-facial tension, wettability, permeability, viscosity just to mention but a few. The aim of EOR is to alter these parameters in several beneficial ways so as to extract the residual oil.

2.2 Some conventional EOR methods and mechanisms

There are several EOR techniques known to recover the residual oil. The type used for a specific reservoir mainly depends on the properties of the reservoir. This aspect brings to light some commonly used EOR techniques.

2.2.1 Gas Injection

It is called miscible flooding [5] and is the most commonly used method. It is a general term for injection processes that introduce miscible gases into the reservoir. A miscible displacement process maintains reservoir pressure and improves oil displacement because the inter-facial tension between oil and water is reduced. This refers to removing the interface between the two interacting fluids. This allows for total displacement efficiency.
Gases used in this process include carbon-dioxide (CO_2) and nitrogen (N_2). The fluid most commonly used for miscible displacement is carbon-dioxide since it has the tendency to reduce the oil viscosity and is less expensive than liquefied petroleum gas. Oil displacement by carbon-dioxide injection relies on the phase behaviors of the mixtures of these two gas and the crude. These behaviors are strongly dependent on reservoir temperature, pressure and crude oil composition. As oil and gas have a cognate symbiosis in the same structural trap, their physical and chemical properties are similar. As such, the gas drive oil method has the potential to deliver better displacement process efficiency and higher recovery rates than other techniques. However, this theory is relevant only under specific reservoir conditions. If these specific conditions are present, then the volume expansion of

the injected gas, which acts to move the oil, takes precedent over the smaller chemical reactions from the gas drive process at the oil and gas interface.

2.2.2 Chemical flooding

In a chemical flood, chemicals are injected with the water flood to improve the displacement efficiency [5]. A chemical solvent is specially developed for adaptation to the specific structural characteristics and physiochemical properties of a reservoir.
After injecting with water, chemical reactions form new chemical sediment, which can reduce the contradiction between layers, increase volume and amount of water injected. This can improve the degree to which reserves can be recovered, while improving production efficiency.
However, this type of chemical reaction would take place in a poor reservoir so it will also produce oil pollution and the capacity for water absorption would be damaged. Most wells cannot achieve a satisfactory result using this method, making it counterproductive, with the negative effects outweighing the benefits.

2.2.3 Thermal recovery

Thermal method raises the temperature of regions of the reservoir to heat the crude oil in the formation and reduces its viscosity or vaporise part of the oil thereby decreasing the mobility ratio. It includes the injection of hot water, steam and other gases or by conducting combustion *in situ* of oil or in gas.
The increase in heat reduces the surface tension, increases the permeability of the oil and improves the reservoir seepage conditions [5]. The heated oil may also vaporise and then condense, forming improved oil.
This approach however, requires substantial investment in special equipment. Due to the heat effect, this method causes severe damage to the underground well structure, as well as poses safety risks in the larger production process. For these reasons, the method is not generally used.

2.2.4 Polymer flooding

Polymer flooding is also widely used as gas flooding. It is used to retrieve oil left behind after conventional recovery processes [5]. It is an augmented water flooding technique introduced in the 1960's, mainly used for heterogeneous reservoirs, to retrieve oil after areas in the reservoir with high permeability have been highly water flooded.
It is a method in which high-molecular-weight polyacrylamides are injected into the water, so as to increase the viscosity of fluid, improve volumetric sweep efficiency and thereby further increasing the oil recovery factor.
When oil is displaced by water, the oil/water mobility ratio is so high that the injected water fingers through the reservoirs. By injecting polymer solution into reservoirs, the oil/water mobility ratio can be much reduced, and the displacement front advances evenly to sweep a larger volume. The viscoelasticity of polymer solution can help displace oil remaining in micro pores that cannot be otherwise displaced by water flooding."

Most of the EOR methods discussed above are known to be costly and task challenging since most of them involves a significant change in the reservoir condition and others even cause a permanent damage to the reservoir. Until recently, the use of microbial to enhance the recovery of the residual oil is emerging as a cheap and effective EOR method [6]. They are cheap in that these microbial are found everywhere on earth. Research has shown that they are among the first life forms to appear on earth and are present in most of its' habitats [7]. They inhabits the soil, water, acidic hot springs, radioactive waves and deep portions of the earth's crust. It is worth noting that about 40 millions of microbes can be found in a gram of soil and a million cells of microbes are contained in a milliliter of fresh water. With approximately 5 x 10^{30} bacteria living on earth, forming a biomass which exceeds that of all plants and animals [8], it is undeniable that they are found everywhere on planet earth.

2.3 The MEOR method

This is a biological method which involves injecting bacteria into the oil reservoir to improve the recovery efficiency [5]. Experimental results using a particular species in a reservoir have shown that through the metabolism of large population bacteria, large amounts of organic acids can be produced. These organic acids may act to restore vitality to an ageing well, increase its productivity and thereby acting to induce a substantial increase in oil recovery.
Compared with most other EOR methods, MEOR is emerging as the cheapest way to recover the residual oil due to its' low economical cost, low risk for the personnel and a little destroyer (if any) to the environment.

2.3.1 Types of MEOR

There are three types of MEOR processes known to recover oil from reservoirs [9]. The first type is similar to conventional chemical flooding. Metabolites with favorable oil-displacing properties are generated as bacteria are grown *ex situ* on suitable nutrients. Fermentation broth with (or without) cells removed is injected into candidate reservoirs to displace oil. The second type makes use of the *in situ* fermentation of nutrients(e.g Molasses) injected into the reservoir. Potential bacteria species are inoculated to carry out the desired biological conversions. Metabolites and biogas are generated in place, allowing for the release of oil trapped in the pores of the reservoir. The third type is similar to the second type but no nutrient is supplied *ex situ* [9]. The bacteria species injected into the reservoir must be capable of utilizing hydrocarbons in the reservoir to generate metabolites *in situ*.

2.3.2 General processes of MEOR

The processes generally involves:

- Injection of microbial along with nutrients into the well and closing for approximately 20 days.
- The microbial then propagates and produce polymers, gases, surfactants and organic acid (their metabolites)
- These metabolites then aid in propagating oil by changing both the physical properties of the rock and crude oil itself.
- The gas **(carbon-dioxide and methane)** restore the gas drive phenomenon of the oil pushing it to the mouth of the well.

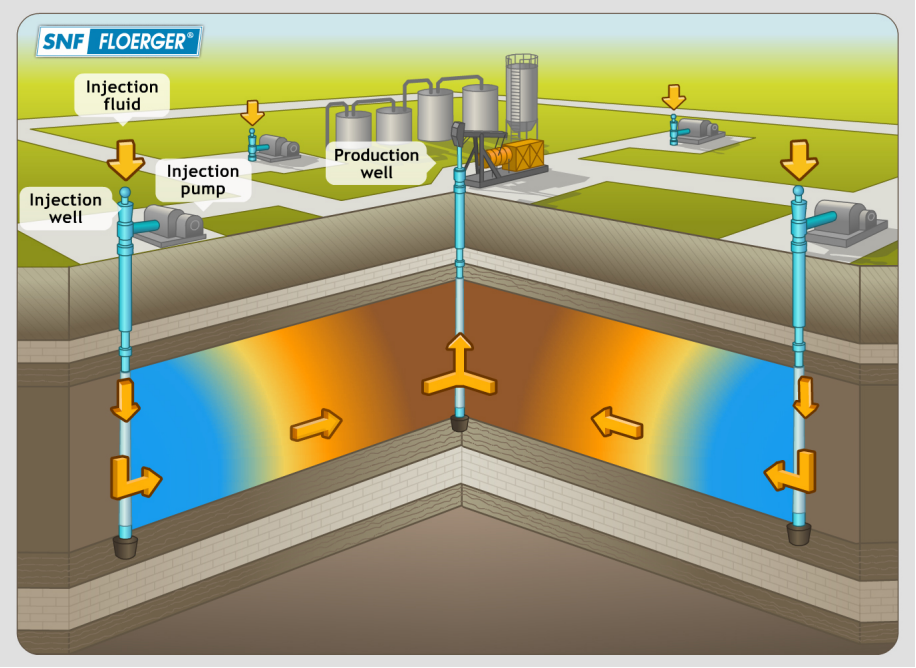

FIGURE 2.1: Processes of MEOR

2.3.3 By-Products of microbial and their effect on the rock and oil

Below is table 2.1 showing details of the metabolites of microbial and their numerous effects on the crude oil and the reservoir rock.

By-Products	**Effects**
Acids	• Modification of reservoir rock. • Improvement of porosity and permeability. • Reaction with calcareous rocks and CO_2 production.
Biomass	• Selective or non selective plugging. • Emulsification through adherence to hydrocarbons. • Modification of the solid surfaces. • Degradation and alteration of oilfields. • Reduction of oil viscosity and soil pour point. • Desulfurization of oil.
Gasses (CO_2, CH_4, H_2)	• Reservoir repressurization. • Oil swelling. • Viscosity reduction. • Increase of permeability due to solubilization of carbonate rocks by CO_2. • Reduction of oil viscosity and soil pour point. • Desulfurization of oil.
Surface active agents	• Lowering of inter-facial tension. • Emulsification.

TABLE 2.1: By-Products effects on rock and oil

2.3.4 Advantages of MEOR method

The merits of using MEOR are numerous and this aspect of the thesis brings to light some of the major advantages. Firstly, It is a fact that microbes live almost everywhere and the fact that they feed on themselves and other nutrients such as molasses, makes the use of MEOR relatively cheap as compared to other enhanced methods. Secondly, no capital expenditure is required for its' treatment, making it economically attractive for marginal producing wells. Also, during the implementation of MEOR activities, only minor modifications to the field facilities are required and results are mostly realized within two to three weeks after the treatment. Again, the operations can be implemented on small pilot areas of about 5 - 10 wells. Furthermore, MEOR has been proven to be a fast and simple application commercially. Finally, it is environmentally friendly in that no harsh chemicals or additives are used as in the case of most other EOR methods since it utilizes indigenous micro-organisms. In General, this method increases oil recovery factor and thus life of the field is extended for years and thereby reducing production decline. These amongst others makes this method phenomenal.

2.3.5 Problems of MEOR method

In spite of its' numerous advantages, MEOR technique faces some problems which are outlined in (Lazar, 2007). To begin with, microbes produce H_2S and SO_2 causing bio-corrosion of the equipment and contamination of ground water. To add to that, in the transportation process, injectivity of microbes is lost due to microbial plugging of the well-bore; thus, dispersion or transportation of all necessary components to the target zone is of much concern and if this is not properly addressed, the whole notion of using microbes to enhance the recovery of the residual oil will never materialize.

Another major concern is the optimization of the desired *in-situ* metabolic activity due to the effect of variables such as PH, temperature, salinity, and pressure for any *in-situ* MEOR operation. This leads to another problem being isolation of microbial strains, adaptable to the extreme reservoir conditions of PH, temperatures, pressure and salinity (Sen, 2008).

Finally, the low *in-situ* concentration of bacteria metabolites is a headache.

In spite of the various advantages of MEOR over other EOR methods, MEOR has not gained credibility in the oil industry because the value of MEOR can only be determined by the results of field trials. Again, MEOR's literature is mainly based on laboratory data and a shortage of field trials can be seen in this field. Also, because of reservoir heterogeneity, it is so difficult to extrapolate laboratory results into what is to be expected in the field or predict what will happen in a new field based on the results obtained from another field. Furthermore, few of the tests explain the mechanisms of oil recovery or offer a reasonable analysis of the application outcome. In addition, as (Moses, 1991) pointed out, the follow-up time of most field trials is not long enough to determine the long-term effects of the process. Finally, the precise mechanisms of in-situ MEOR operations are still unclear; thus more research is required in this field (Xu and Lu, 2011).

Chapter 3

Mathematical model

3.1 Two-phase model

This section presents the models and solution algorithms for the saturation and pressure distributions in a two-phase flow through a porous media. The mathematical model, which was developed from the popular Darcy's equation and the continuity equation, contains a substance source/sink term. Using the finite volume discretization scheme, the implicit pressure explicit saturation (IMPES) method was used to solve for pressure and saturation. The implementation was carried out in Matlab.

We note that the relative permeabilities and capillary pressure are functions of the fluid saturation.

The two main dependent variables of interest in two- phase flow in porous medium are saturation and pressure. Saturation is the ratio of the volume that a fluid occupies to the pore volume of the porous medium. The relative amounts of oil, gas or water that will flow when more than one phase is present in a porous medium are dependent on the individual phase saturation. On the other hand, reservoir pressure is used for characterizing a reservoir, estimating its oil capacity and predicting its future behavior. The production of oil and water in a well is a function of the reservoir pressure, which depends on the amount of oil and water in the reservoir, which on its part, is described by the saturation (Craft and Hawkins, 1991).

This thesis therefore, models a two-phase flow in a porous media with a source/sink

term, for the determination of the saturation and pressure distributions. The governing equations are formulated in one-dimension for the saturation and pressure respectively. Although many reservoirs are modeled as two-dimensional space coordinates (Blunt, 2001) due to the fact that petroleum reservoirs are usually more permeable in the horizontal direction than in the vertical direction, this research is limited to just one-dimension.

3.1.1 The governing equations

In the absence of hydrodynamic dispersion, the Darcy's equation (3.1) is written to relate the superficial velocity of the simultaneous flow of each phase to the pressure gradient of the phase:

$$\overrightarrow{U}_{\alpha} = -\frac{K_{r\alpha}\hat{K}}{\mu_{r\alpha}}\left(\nabla P_{\alpha} + \rho_{\alpha}\overrightarrow{g}\right) \tag{3.1}$$

for

$$\alpha = \{Oil(o), Water(w)\}$$

where $\overrightarrow{U}$ $[m/s]$ is the production by cross sectional area of the flow; P [Pa] is the fluid pressure; g [m/s^2] is the acceleration due to gravity; $\hat{K}[m^2]$, $K_{r\alpha}$, μ[pas] and ρ[kg/m^3] are the single phase permeability, relative permeability, viscosity and density respectively.

Due to the surface tension and curvature of the inter-phase between the two phases, one phase referred to as the wetting phase being water tends to wet the porous medium more than the other phase, referred to as the non-wetting phase being oil (Xue, 2004). Since the void volume is completely occupied by the two fluid, the following equation applies for the saturations:

$$S_w + S_o = 1 \tag{3.2}$$

The pressures of the two phases are related to each other through the capillary pressure $P_c(S_w)$, (Xue, 2004) given by;

$$P_o - P_w = P_c(S_w). \tag{3.3}$$

By relating the effective permeabilities $\hat{K_o}$ and $\hat{K_w}$ to the single phase permeability $\hat{K}$, the relative permeabilities K_{ro} and K_{rw} can be defined as:

$$\hat{K_w} = K_{rw}\hat{K}$$

$$\hat{K_o} = K_{ro}\hat{K}.$$

The relative permeabilities are empirically taken to be functions of saturation and are assumed to be independent of direction (Aziz and Settari, 1979). From the continuity equation, we have:

$$\frac{\partial\left(\rho_\alpha S_\alpha \phi\right)}{\partial t} + \nabla \cdot \left(\rho_\alpha \overrightarrow{U}_\alpha\right) = F_{v,\alpha}\ , \quad \alpha = w, n \tag{3.4}$$

Where ϕ[-] is the porosity or void fraction of the porous media and $F_{v,\alpha}$ [kg/$m^3 s$] represent the sink or source capacities for each respective phases and t[s] is the production time.

Equations (3.4) represent the mathematical model for the flow of two immiscible phases in porous media. In order to solve it for the transient saturation and pressure of each phase, the following additional information is to be provided:

- Capillary pressure and relative permeabilities as functions of saturation.
- Appropriate boundary and initial conditions.
- The porosity and fluid properties (densities and viscosities).

In this model, we assume that densities and porosity are constant and also we neglect gravity since a transverse one dimensional flow is considered. With these assumptions, substituting the Darcy law equation (3.1) into the continuity equation for each phase results in;

$$\frac{\phi\partial\left(S_w\right)}{\partial t} - \nabla \cdot \frac{K_{rw}\hat{K}}{\mu_w}(\nabla P_w) = \frac{F_{v,w}}{\rho_w} \tag{3.5}$$

$$\frac{\phi\partial\left(S_o\right)}{\partial t} - \nabla \cdot \frac{K_{ro}\hat{K}}{\mu_o}(\nabla P_o) = \frac{F_{v,o}}{\rho_o}. \tag{3.6}$$

It is worth noting that equations (3.2), (3.3), (3.5) and (3.6) give the fully coupled equations for the two phase model of oil and water. In order to solve them, these

equations have to be either coupled or decoupled into pressure and saturation equations depending on the formulation and the numerical method used.

Making S_o the subject in equation (3.2) and substituting into equation (3.6) gives;

$$\frac{\phi\partial\left(1-S_w\right)}{\partial t}-\nabla\cdot\frac{K_{ro}\hat{K}}{\mu_o}(\nabla P_o)=\frac{F_{v,o}}{\rho_o} \tag{3.7}$$

To eliminate the saturations, we add equations (3.5) and (3.7). This results in:

$$-\nabla\cdot\hat{K}[\lambda_w\nabla P_w+\lambda_o\nabla P_o]=F_{v,T} \tag{3.8}$$

Where,

$$\lambda_\alpha=\frac{K_{r\alpha}}{\mu_\alpha},\qquad \alpha=w,o \tag{3.9}$$

and

$$F_{v,T}=\frac{F_{v,o}}{\rho_o}+\frac{F_{v,w}}{\rho_w}. \tag{3.10}$$

Equation (3.9) is called the phase mobility whilst equation (3.10) is the total source or sink term

Various formulations such as the mean value formulation, the global pressure formulation and the fractional flow formulation can be used. In this research, we make use of only the mean value formulation.

3.1.2 The mean value formulation

$$\overline{P} = \frac{P_o + P_w}{2}. \tag{3.11}$$

From equations (3.3) and (3.11), we have

$$P_o = \overline{P} + \frac{1}{2}P_c(S_w) \tag{3.12}$$

$$P_w = \overline{P} - \frac{1}{2}P_c(S_w). \tag{3.13}$$

Substituting (3.12) and (3.13) into (3.8) gives,

$$-\nabla \cdot \hat{K}\left[\lambda_w \nabla\left(\overline{P} - \frac{1}{2}P_c(S_w)\right) + \lambda_o \nabla\left(\overline{P} + \frac{1}{2}P_c(S_w)\right)\right] = F_{v,T}. \tag{3.14}$$

Now, using $\overline{P}$ and S_w as primary variables, we solve equations (3.14) and (3.5) using the finite volume discretization scheme. We note that these two equations are nonlinear partial differential equations. Although Newton's fix point iterative solver can be used to solve it nonlinearly, this thesis employed the IMPES method which takes care of the nonlinearity. For an alternative robust implicit discretization approach to these equations, we refer to [32]. For our system of equation under consideration, we have:

$$\begin{cases} -\nabla \cdot \hat{K}\left[\lambda_w \nabla\left(\overline{P} - \frac{1}{2}P_c(S_w)\right) + \lambda_o \nabla\left(\overline{P} + \frac{1}{2}P_c(S_w)\right)\right] = F_{v,T} \\ \\ \frac{\phi \partial(S_w)}{\partial t} - \nabla \cdot \hat{K}\left[\lambda_w \nabla(\overline{P} - \frac{1}{2}P_c(S_w))\right] = \frac{F_{v,w}}{\rho_w} \\ \\ + \text{ appropriate boundary conditions} \\ \\ + \text{ appropriate initial conditions} \end{cases} \tag{3.15}$$

Simplifying equation (3.15) and applying boundary and initial conditions, we have;

$$\begin{cases} -\nabla \cdot \hat{K}\left[\lambda_T \nabla(\overline{P}) + \frac{1}{2}\lambda_d \nabla\left(P_c(S_w)\right)\right] = F_{v,T} \\ \\ \frac{\phi \partial(S_w)}{\partial t} - \nabla \cdot \hat{K}\left[\lambda_w \nabla(\overline{P} - \frac{1}{2}P_c(S_w))\right] = \frac{F_{v,w}}{\rho_w} \\ \\ \quad + \text{appropriate boundary conditions} \\ \\ \begin{array}{c} S_w(x,0) = S_w^0(x) \\ \overline{P}(x,0) = \overline{P}^0(x) \end{array} \end{cases} \tag{3.16}$$

Where, $\lambda_T = \lambda_w + \lambda_o$ being the total mobility and
$\lambda_d = \lambda_o - \lambda_w$.

3.2 Microbial transport mechanisms in porous media

The main goal of MEOR is to recover the residual oil by the use of microbial. As earlier noted, the residual oil left after the application of primary and secondary means of oil production is about 35-55%. The thesis at this stage brings to bare the transport mechanisms that may describe some basic mechanisms regulating the dynamics and interaction between microbial organisms and the porous medium with divers compositions of fluids [21]. We recall that one of the major challenges facing MEOR processes is transport: thus, getting the microbial to hit the target zones. Anaerobic microbial organisms such as *Clostridium, Bacillus, Pseudomonas* just to mention but a few are normally found in subsurface porous medium. If we however inject oxygen into the reservoir, aerobic organisms may also survive. Thus, we often find a large variation of microbial types in such environment. The microbial organisms of interest considered in this work are bacteria. Therefore we use this term for the organisms even if the more general term microbial organisms could have been used.

3.2.1 Transport equations

With the assumption that the porous medium contains some amount of water, let C be the concentration of the bacteria in water. From [22] and [23], a simple way to model spatial and temporal variation of C at macro scale is by the simple advection-dispersion equation (3.17)

$$\frac{\partial C}{\partial t} = D\frac{\partial^2 C}{\partial x^2} - \nu\frac{\partial C}{\partial x} \tag{3.17}$$

in which D is the hydrodynamic dispersion coefficient, and ν stands for the velocity of the water driven bacteria.

3.2.2 Adsorption

During transport, a fraction of the bacteria will be adsorbed by the solid surface. Denoting the attached bacteria concentration by ψ, a general governing equation

for transport of bacteria in water-saturated porous media is [[22], [23]]:

$$\frac{\partial C}{\partial t} + \frac{\rho_b}{\phi}\frac{\partial \psi}{\partial t} = D\frac{\partial^2 C}{\partial x^2} - \nu\frac{\partial C}{\partial x} \tag{3.18}$$

where ϕ is the porosity and ρ_b is the (dimensionless) dry bulk density.

This thesis does not take into consideration certain factors such as equilibrium formulations in which retardation growth will be taken care of and also adsorptions involving kinetics.

3.2.3 Growth and decay

The growth and decay of the bacteria are not taken into account in the transport equations (3.17) and (3.18). To make way for them, we include a source term q in the transport equation:

$$\frac{\partial C}{\partial t} + \frac{\rho_b}{\phi}\frac{\partial \psi}{\partial t} = D\frac{\partial^2 C}{\partial x^2} - \nu\frac{\partial C}{\partial x} + q \tag{3.19}$$

where q represents the rate of growth or decay, depending on its sign. For simple systems, a common choice for the source term q is the Monod equation [26] which is given by

$$q = \varphi_{max}\frac{C}{K_c + C} \tag{3.20}$$

where:

q is the specific growth rate of the microorganisms φ_{max} is the maximum specific growth rate of the microorganisms, C is the concentration of the limiting substrate for growth and K_c is the "half-velocity constant"(the value of C when $\frac{q}{\varphi_{max}} = 0.5$). φ_{max} and K_c are empirical coefficients to the Monod equation.

For multicomponent systems, the source term q_i for the component i will depend on the concentrations of one or more of the other components, and on chemical reactions. Denoting the chemical reaction by R and assuming that the bacteria are living in the water, the conservation based equations for the concentration of a component i in water (C_i^w) are then given as

$$\frac{\partial(S_w \phi C_i^w)}{\partial t} + \frac{\rho_b}{\phi}\frac{\partial \psi}{\partial t} - D\frac{\partial^2 C_i^w}{\partial x^2} + \nu_i \frac{\partial C_i^w}{\partial x} = q_i^w + R(C_i^w) \tag{3.21}$$

We note that equation (3.21) forms part of our model problem equation (3.16)

3.2.4 Exponential growth

We consider a stationary system, and assume that the concentrations of the essential nutrients for a specific bacteria, remain sufficiently high. The number $n(t)$ of bacteria in the system will then increase exponentially: $n(t) = n_0 b^{t/T}$ where $n_0 = n(0)$ is the initial number of bacteria, b is the growth factor, and T is the time needed for the number $n(t)$ to increase by a factor b.

The discretization of the main mathematical models equations (3.16) and (3.21) are discussed in chapter 4 of this thesis.

Chapter 4

Numerical modeling

The term numerical modeling often refers to solving a partial or an ordinary differential equation. With regards to our set of coupled nonlinear partial differential equation we need to solve it numerically. The finite difference method described in [12] and the two point flux approximation [24] which is a control volume method are used. This aspect of the thesis brings to light the theoretical background for the discretization, sets up the discretization schemes for the equations and show how they are decoupled.

4.1 Grid

Most continuous partial differential equations have their solutions in the infinite dimensional space hence a solution should be sought for in the finite dimensional space. This brings to bear the concept of discretization. Thus, our problem has to be solved numerically by discretizing it. The same accounts for if you want to represent a mathematical function $f(x)$ numerically, you must first define the points x_i where the function is evaluated. Defining these points simply implies to define a suitable grid on the domain of the function.
The way the grids are defined can be thought of as dividing the interval into cells with walls separating the cells. From a two - dimensional perspective, the grids are generated by putting out several points in the domain, and then connecting the points by straight lines not intersecting each other. When we look at the grids as containing cells, the lines are the cell walls whilst the grid points are the corners of the cells. We then can choose the points x_i to be the same as the grid points, or

we can let the points x_i be the middle points of the cells, giving us a cell-centered grid [10], see fig. 4.1.

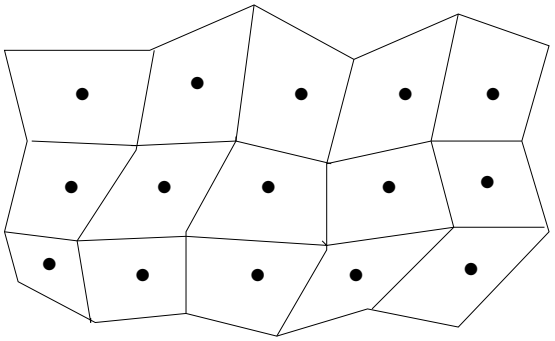

FIGURE 4.1: An example of a cell-centered grid in 2-D

Control-volume method mostly uses a cell-centered grid. Usually, to define the points x_i for a cell-centered grid, one needs to divide the interval into cells first, then find the middle point of the cells and let them be the points x_i [10]. But for an equidistant one-dimensional grid, it does not matter if one defines the discretization points x_i or the walls of the cells first.

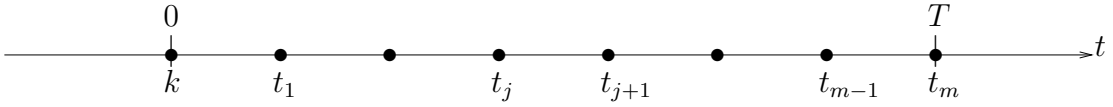

FIGURE 4.2: Equal distant time discretization

Our problem has to be discretized in both space and time. The time interval is [0 , T], thus starting from initial time $t_o = 0$ to final time $t_m = T$. The size of the time steps are given by $\triangle t_j = t_j - t_{j-1}$. We have equal distance time interval, where time step size is constant. Thus, $\triangle = \tau$ for $j = 0, ..., m$. Hence, τ is found from $\tau = \frac{T}{m}$.

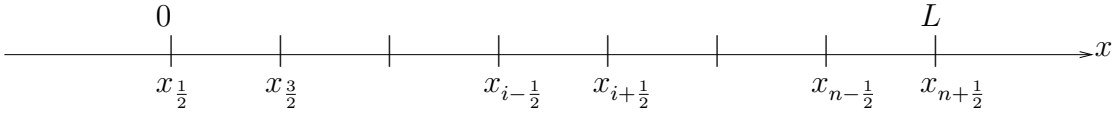

FIGURE 4.3: Space interval divided into equal sized cells

We again use the control-volume method in space. Thus, we discretize the space interval [0 , L] into a cell-centered grid. For convenience regarding the spacing, we consider equal distant grid. We then start by dividing the interval [0 , L] into n equal cells. The walls of the cells are then given by $x_{i+\frac{1}{2}} = ih$ for $i = 0, ..., n$ where $h = x_{i+\frac{1}{2}} - x_{i-\frac{1}{2}} = \frac{L}{n}$. Then $x_{\frac{1}{2}} = 0$ and $x_{i+\frac{1}{2}} = L$ gives the boundaries of the domain, see fig. 4.3.

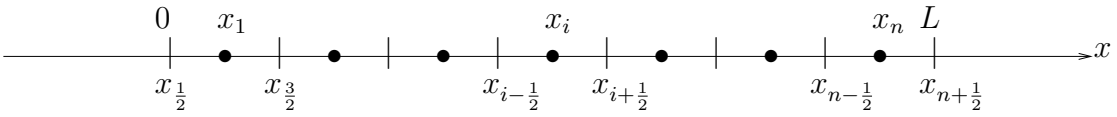

FIGURE 4.4: Cell-centered space discretization.

After dividing the space intervals into cells, we take the middle points of the cells to be the grid points $x_1, x_2, ..., x_n$; see figure 4.4. The reason being that, since we have an equal distant grid, the distance between the neighboring grid points will be the same as the size of the cells, $\triangle x_i = x_{i+1} - x_i = h$. Then $x_1 = \frac{h}{2}$ and $x_i = ih - \frac{h}{2}$ for $i = 0, ..., n$. The last grid point is $x_n = nh - \frac{h}{2} = L - \frac{h}{2}$.

4.2 Spatial discretization

This aspect looks at the spatial discretization techniques since the only discretization technique used for the time is the backward Euler method. Several discretization techniques exist for discretizing the spatial component of a partial differential equation but the method used mostly in this thesis is the two point flux approximation, being a control volume-method. Since this work is limited to one-dimension, this two point flux approximation is equivalent to the finite difference method for a cell centered grid.

4.2.1 The finite difference methods

This method has its base from the Taylor series expansion for $u(x + h) = u(x_{i+1})$ and $u(x-h) = u(x_{i-1})$ and is the most elementary spatial discretization technique. Although not widely used today due to its inability to contain the conservative property required for most problems, it is widely described in books on numerical analysis, such as [10, 16–18]. The Taylor series and finite difference method are

also the bases for the time discretization equation.
From the Taylor series

$$u(x_{i+1}) = u(x_i) + hu'(x_i) + \frac{h^2}{2}u''(x_i) + \frac{h^3}{3!}u'''(x_i) + ..., \tag{4.1}$$

we get the forward difference approximation for the first derivative,

$$u'(x_i) = \frac{u(x_{i+1}) - u(x_i)}{h} + O(h) \tag{4.2}$$

The order of the method is given by the term $O(h)$. It represents the terms which are truncated from the Taylor series and it is that which determines the order of convergence.
In the same vein, we get the backward difference approximation

$$u'(x_i) = \frac{u(x_i) - u(x_{i-1})}{h} + O(h), \tag{4.3}$$

from

$$u(x_{i-1}) = u(x_i) - hu'(x_i) + \frac{h^2}{2}u''(x_i) - \frac{h^3}{3!}u'''(x_i) + ..., \tag{4.4}$$

From equations (4.2) and (4.3), it is seen that both forward and backward difference approximations are of order $O(h)$, making them not to be the best.
Now, subtracting equation (4.4) from equation (4.1) gives the central difference approximation scheme

$$u'(x_i) = \frac{u(x_{i+1}) - u(x_{i-1})}{2h} + O(h^2), \tag{4.5}$$

which is a better approximation.
Finding an approximation for the second derivative, we use

$$\frac{u(x_{i+1}) - u(x_i)}{h} = u'(x_i) + \frac{h}{2!}u''(x_i) + \frac{h^2}{3!}u'''(x_i) + \frac{h^3}{4!}u''''(x_i)... \tag{4.6}$$

$$\frac{u(x_i) - u(x_{i-1})}{h} = u'(x_i) - \frac{h}{2}u''(x_i) + \frac{h^2}{3!}u'''(x_i) - \frac{h^3}{4!}u''''(x_i)... \tag{4.7}$$

Subtracting equation (4.7) from equation (4.6) results in

$$u''(x_i) = \frac{u(x_{i+1}) - 2u(x_i) + u(x_{i-1})}{h^2} + O(h^2) \tag{4.8}$$

which gives the central difference approximation scheme for the second derivative $u''(x_i)$.

Although this method is very simple to implement, its major challenge is seen when applied to very complex geometry. Also, due to where it stems from, makes it not to have the conservative property.

4.2.2 The two point flux approximation

We consider the ordinary stationary differential equation

$$-(K(x)P_x)_x = Q(x) \tag{4.9}$$

where
$K(x)$ denote the permeability, $Q(x)$ the source term and $P_x = \frac{\partial p}{\partial x}$.

Assume

$$q = -K(x)P_x. \tag{4.10}$$

Then from equations (4.9) and (4.10), we have

$$-q_x = Q(x). \tag{4.11}$$

We want to solve equation (4.10) for q. We first begin to discretize it using fig.4.5 below

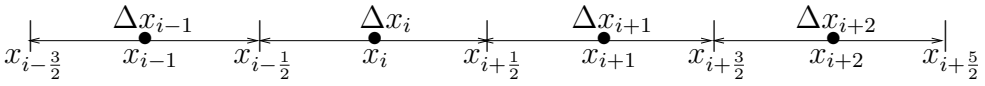

FIGURE 4.5: Cell centered grid with points x_i and the cell walls $x_{i+\frac{1}{2}}$

.

The grid points x_i for $i = 0, 1, 2, ..., n$ are the middle points of the cells. The walls are of cell with mid point x_i given by $x_{i-\frac{1}{2}}$ and $x_{i+\frac{1}{2}}$. Integrating equation (4.11) over each cell, we get;

$$-\int_{x_{i-\frac{1}{2}}}^{x_{i+\frac{1}{2}}} q_x dx = \int_{x_{i-\frac{1}{2}}}^{x_{i+\frac{1}{2}}} Q(x)dx$$

which results in

$$q_{i+\frac{1}{2}} - q_{i-\frac{1}{2}} = \int_{x_{i-\frac{1}{2}}}^{x_{i+\frac{1}{2}}} Q(x)dx. \tag{4.12}$$

We now seek to find an expression for $q_{i+\frac{1}{2}}$ by K and P . This is done by re-writing equation (4.11) as

$$P_x = -\frac{q}{K(x)}. \tag{4.13}$$

If we now integrate equation (4.13) from the middle point x_i to the middle point x_{i+1}, we get

$$\int_{x_i}^{x_{i+1}} P_x dx = -\int_{x_i}^{x_{i+1}} \frac{q}{K(x)} dx$$

$\Longrightarrow$

$$P_{x_{i+1}} - Px_i = -q_{i+\frac{1}{2}} \int_{x_i}^{x_{i+1}} \frac{1}{K(x)} dx$$

hence

$$q_{i+\frac{1}{2}} = -\frac{P_{x_{i+1}} - Px_i}{\int_{x_i}^{x_{i+1}} \frac{1}{K(x)} dx}.$$

We now need an approximation for the integral

$$\int_{x_i}^{x_{i+1}} \frac{1}{K(x)} dx$$

from grid point x_i to grid point x_{i+1}. These are the middle points in two neighboring cells, thus, we integrate over two cells. We assume that $K(x)$ is constant on each cell, denoted by the values at the grid point, $K_i \approx K(x_i)$. We let Δx_i denote the distance between the walls of the cell. Thus, $\Delta x_i = x_{i+\frac{1}{2}} - x_{i-\frac{1}{2}}$. We approximate the integral by taking the average over the two cells involving x_i and x_{i+1}.

$\Longrightarrow$

$$\int_{x_i}^{x_{i+1}} \frac{1}{K(x)} d_x = \frac{1}{2} \left(\frac{\Delta x_{i+1}}{K_{i+1}} + \frac{\Delta x_i}{K_i} \right).$$

Thus we get the following expression

$$q_{i+\frac{1}{2}} = -\frac{P_{i+1} - P_i}{\frac{1}{2} \left(\frac{\Delta x_{i+1}}{K_{i+1}} + \frac{\Delta x_i}{K_i} \right)}$$

which becomes

$$q_{i+\frac{1}{2}} = -a_{i+1}(P_{i+1} - P_i) \tag{4.14}$$

if we let

$$a_i = \frac{1}{\frac{1}{2}\left(\frac{\Delta x_i}{K_i} + \frac{\Delta x_{i-1}}{K_{i-1}}\right)}.$$

This holds for a non-equidistant cell centered grid. For equidistant cell-centered grid, we have $\Delta x_i = \Delta x_{i-1} = h$ for $i = 0, ..., n$. This gives

$$a_i = \frac{1}{\frac{h}{2}\left(\frac{1}{K_i} + \frac{1}{K_{i-1}}\right)} \tag{4.15}$$

In this thesis, only equidistant cell-centered grids are considered. Now, substituting for q, equation (4.12) becomes

$$\frac{P_i - P_{i-1}}{\frac{h}{2}\left(\frac{1}{K_i} + \frac{1}{K_{i-1}}\right)} - \frac{P_{i+1} - P_i}{\frac{h}{2}\left(\frac{1}{K_{i+1}} + \frac{1}{K_i}\right)} = \int_{x_{i-\frac{1}{2}}}^{x_{i+\frac{1}{2}}} Q(x)d_x \tag{4.16}$$

which can be written as

$$a_i(P_i - P_{i-1}) - a_{i+1}(P_{i+1} - P_i) = b_i \tag{4.17}$$

where b_i is defined as

$$b_i = \int_{x_{i-\frac{1}{2}}}^{x_{i+\frac{1}{2}}} Q(x)d_x. \tag{4.18}$$

Transposing equation (4.17), we have

$$-a_iP_{i-1} + (a_i + a_{i+1})P_i - a_{i+1}P_{i+1} = b_i \tag{4.19}$$

for $i = 1, ..., n$. Thus, we have a system of n equations. The unknown are $[P_o, P_1, ..., P_n, P_{n+1}]$. That is, there are $n + 2$ unknown. In order to obtain a unique solution, we need an additional boundary conditions. In this thesis, two commonly boundary conditions are discussed.

4.2.3 Dirichlet boundary conditions

Under this system of boundary condition, the value of the unknown function is specified at end point of the domain. With regards to our stationary one-dimensional problem (4.9) on the domain [0 , L] with the unknown pressure $p = p(x)$. The Dirichlet boundary conditions can be given as

$$p(0) = p_0 \tag{4.20}$$

and

$$p(L) = p_L. \tag{4.21}$$

Since we are using the cell-centered grid in figure 4.5, when the problem is discretized,

$$p_{\frac{1}{2}} = p_0,$$

and

$$p_{n+\frac{1}{2}} = p_L.$$

It is however not a straight forward issue in handling Dirichlet boundary conditions for a cell-centered gird and we need to find a trick in doing it. It is quite straight forward in the case of vertex centered grid since the boundary points will coincide with the grid points at the end.

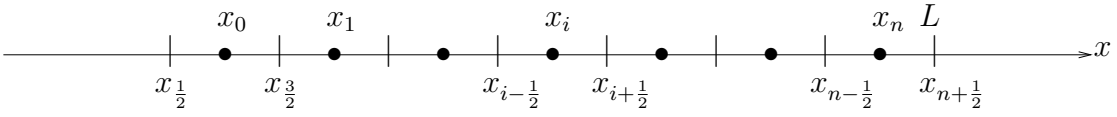

FIGURE 4.6: Dirichlet boundary conditions for cell-centered grid by adding ghost cells at the ends of the interval.

In the book by J. W. Thomas [25], two ways of handling Dirichlet boundary conditions are presented for cell-centered grids. One way is simply by adding ghost cells at the ends of the interval as shown in figure 4.6. Then we assume that the Dirichlet boundary conditions are prescribed at the ghost cells and we discretize in the first and last cells as done in the figure above. This will result in additional grid points x_0 and x_{n+1} and we assume

$$p_0 = p_o,$$

and

$$p_{n+1} = p_L.$$

In [25], it is noted to be a first order approximation making it not be sufficient if the solution largely depends on the boundary conditions. The second simplest way is to add half cells at the ends of the intervals as shown in figure 4.7. This thesis however makes use of the first approach only.

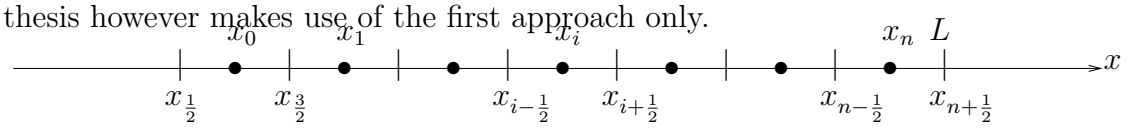

FIGURE 4.7: Dirichlet boundary conditions for cell-centered grid by adding half cells at the ends of the interval.

Using the first approach of adding ghost cells normally handle the Dirichlet boundary conditions the same as we would have done for a vertex centered grid. The difference lies in how the grid points x_i are defined and also in the points in which we evaluate the p values. An illustration of how to manage the boundary condition is given below for

$$-\left(Kp_x\right)_x = Q. \tag{4.22}$$

Where we make use of the first approach by adding ghost cells in the ends of the interval. From the discretization of the problem as shown in equation (4.19) results in the system of equations

$$\begin{aligned}
-a_1p_0 + [a_1 + a_2]p_1 - a_2p_2 &= b_1 \\
-a_2p_1 + [a_2 + a_3]p_2 - a_3p_3 &= b_2 \\
&\dots \\
&\dots \\
&\dots \\
-a_{n-1}p_{n-2} + [a_{n-1} + a_n]p_{n-1} - a_np_n &= b_{n-1} \\
-a_np_{n-1} + [a_n + a_{n+1}]p_n - a_{n+1}p_{n+1} &= b_n
\end{aligned}$$

With Dirichlet boundary conditions, we require two boundary conditions $p_0 = p_o$ and $p_{n+1} = p_L$ for the pressure. Moving the boundary terms to the right hand

side of the system of equations results in

$$\begin{aligned}
[a_1 + a_2]p_1 - a_2p_2 &= b_1 + a_1p_o \\
-a_2p_1 + [a_2 + a_3]p_2 - a_3p_3 &= b_2 \\
&... \\
&... \\
&... \\
-a_{n-1}p_{n-2} + [a_{n-1} + a_n]p_{n-1} - a_np_n &= b_{n-1} \\
-a_np_{n-1} + [a_n + a_{n+1}]p_n &= b_n + a_{n+1}p_L.
\end{aligned}$$

Writing this in matrix form implies

$$\mathbf{A} = \begin{pmatrix}
a_1 + a_2 & -a_2 & 0 & . & . & . & 0 \\
-a_2 & a_2 + a_3 & -a_3 & . & . & . & . \\
0 & \ddots & \ddots & \ddots & \ddots & \ddots & . \\
. & \ddots & \ddots & \ddots & \ddots & \ddots & . \\
. & & & \ddots & -a_{n-1} & a_{n-1} + a_n & a_n \\
0 & & 0 & 0 & 0 & -a_n & a_n + a_{n+1}
\end{pmatrix}.$$

and

$$\mathbf{b} = \begin{pmatrix}
b_1 + a_1P_o \\
b_2 \\
b_3 \\
. \\
. \\
. \\
b_{n-1} \\
b_n + a_{n+1}p_L
\end{pmatrix}.$$

which gives the linear system

$$Ap = b$$

for $p = [p_1, p_2, p_3, ..., p_n, p_{n+1}]^T$ which can then be solved by the use of a numerical linear solver.

4.2.4 Neumann boundary conditions

In the case where we have Neumann boundary conditions, the values of the first derivative of the function is specified at the boundaries. Thus, in a one-dimensional case, this boundary condition is given as

$$p_x(0) = p_\alpha \tag{4.23}$$

and

$$p_x(L) = p_\beta. \tag{4.24}$$

From figures [4.4 and 4.6], we again realize that $x_{\frac{1}{2}} = 0$ and $x_{n+\frac{1}{2}} = L$. Since $q_{i+\frac{1}{2}}$ is the expression for the derivative of the pressure p at the cell wall $x_{i+\frac{1}{2}}$, the boundary condition can then be written as

$$q_{\frac{1}{2}} = -\frac{p_\alpha}{\frac{1}{2}\left(\frac{1}{K_0} + \frac{1}{K_1}\right)}$$

and

$$q_{n+\frac{1}{2}} = -\frac{p_\beta}{\frac{1}{2}\left(\frac{1}{K_n} + \frac{1}{K_{n+1}}\right)}$$

With K_0 and K_{n+1} unknown, lets assume that $K_0 = K_1$ and $K_n = K_{n+1}$. Assuming also that we have homogeneous Neumann boundary conditions, that is $p_\alpha = p_\beta = 0$. This then results in

$$q_{\frac{1}{2}} = 0 \tag{4.25}$$

and

$$q_{n+\frac{1}{2}} = 0 \tag{4.26}$$

making the values for K_0 and K_{n+1} to be irrelevant.
Showing also how to deal with Neumann boundary conditions for the discretization of equation (4.9)

$$-(K(x)P_x)_x = Q(x).$$

Using again our previous discretization, from equations (4.12) and (4.18), we have

$$q_{i+\frac{1}{2}} - q_{i-\frac{1}{2}} = b_i,$$

for $i = 1, ..., n$. For the first equation, when $i = 1$, we get

$$q_{\frac{3}{2}} - q_{\frac{1}{2}} = b_i.$$

Here we can insert the boundary condition at $x = 0$ (4.25) which gives

$$q_{\frac{3}{2}} = b_1.$$

Similarly, the last equation for $i = n$, equation (4.26) also becomes

$$-q_{n-\frac{1}{2}} = b_n.$$

Now from the fact that

$$q_{1-\frac{1}{2}} = -ai + 1(p_{i+1} - p_i),$$

the first and the last equation become

$$a_2 p_1 - a_2 p_2 = b_1$$
$$-a_n p_{n-1} + a_n p_n = b_n$$

The rest of the equations follows as before. Again, representing the systems of equations in matrix form

$$Ap = b,$$

where this time

$$\mathbf{A} = \begin{pmatrix} a_2 & -a_2 & 0 & . & . & . & 0 \\ -a_2 & a_2 + a_3 & -a_3 & . & . & . & . \\ 0 & \ddots & \ddots & \ddots & \ddots & \ddots & . \\ . & \ddots & \ddots & \ddots & \ddots & \ddots & . \\ . & & & \ddots & -a_{n-1} & a_{n-1} + a_n & -a_n \\ 0 & & 0 & 0 & 0 & -a_n & a_n \end{pmatrix}.$$

and

$$\mathbf{b} = \begin{pmatrix} b_1 \\ b_2 \\ . \\ . \\ . \\ b_{n-1} \\ b_n \end{pmatrix}.$$

We will again solve the linear system for $\mathbf{p} = [p_1, p_2, p_3, ..., p_n, p_{n+1}]^T$. When we have homogeneous Neumann boundary conditions, $p_\alpha = p_\beta = 0$, and $\mathbf{b}$ simplifies to $\mathbf{b} = [b_1, b_2, ..., b_{n-1}, b_n,]^T$.

4.3 The fully discrete scheme for two-phase flow

We now introduce the discrete form of the continuous problem equation (3.16) by discretizing it using the two point flux approximation. Applying the IMPES results in the decoupled system of equations;

$$\begin{cases} -\nabla \cdot \hat{K}\left[\lambda_T\left(S_w^n\right)\nabla(\overline{P}^{n+1}) + \frac{1}{2}\lambda_d\left(S_w^n\right)\nabla\left(P_c(S_w^n)\right)\right] = F_{v,T} \\ \\ \phi\frac{S_w^{n+1}-S_w^n}{\tau} - \nabla\cdot\hat{K}\lambda_w(S_w^n)\Big(\nabla(\overline{P}^{n+1} - \frac{1}{2}P_c(S_w^n))\Big) = \frac{F_{v,w}}{\rho_w} \\ \\ + \text{ appropriate boundary conditions} \\ \\ S_w(x,0) = S_w^0(x) \\ \overline{P}(x,0) = \overline{P}^0(x) \end{cases}$$

in which the mean pressure is obtained implicitly whilst the water saturation is obtained explicitly.

$\Longrightarrow$

$$S_w^{n+1} = f(S_w^n, \overline{P}^{n+1})$$

and

$$\overline{P}^{n+1} = f(P^{n+1}, S_w^n)$$

The pressure equation above in one dimension is,

$$-\frac{d}{dx}\left[\lambda_T\left(S_w^n\right)\frac{d\overline{P}^{n+1}}{dx} + \frac{1}{2}\lambda_d\left(S_w^n\right)\frac{dP_c\left(S_w^n\right)}{dx}\right] = F_{v,T} \tag{4.27}$$

Discretizing equation (4.27) using the two point flux approximation described above gives

$$-\int_{\Omega_i}\left[\underbrace{\lambda_T\left(S_w^n\right)\frac{d\overline{P}^{n+1}}{dx}}_{A} + \underbrace{\frac{1}{2}\lambda_d\left(S_w^n\right)\frac{dP_c\left(S_w^n\right)}{dx}}_{B}\right]dx = \int_{\Omega_i} F_{v,T}ds \tag{4.28}$$

Recal that from figure 4.5

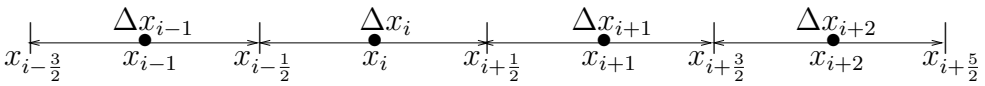

FIGURE 4.8: Cell centered grid with points x_i and the cell walls $x_{i+\frac{1}{2}}$

.

with $\Delta x_i = |\Omega_i| = |x_{i+\frac{1}{2}} - x_{i-\frac{1}{2}}|$.

From equation (4.28), A and B are fluxes and defined by

$$A_{i-\frac{1}{2}} = \lambda_T(S_w^n)\frac{d\overline{P}^{n+1}}{dx}|_{i-\frac{1}{2}}$$

$$A_{i+\frac{1}{2}} = \lambda_T(S_w^n)\frac{d\overline{P}^{n+1}}{dx}|_{i+\frac{1}{2}}$$

$$B_{i-\frac{1}{2}} = \tfrac{1}{2}\lambda_d(S_w^n)\frac{dP_c(S_w^n)}{dx}|_{i-\frac{1}{2}}$$

$$B_{i+\frac{1}{2}} = \tfrac{1}{2}\lambda_d(S_w^n)\frac{dP_c(S_w^n)}{dx}|_{i+\frac{1}{2}}$$

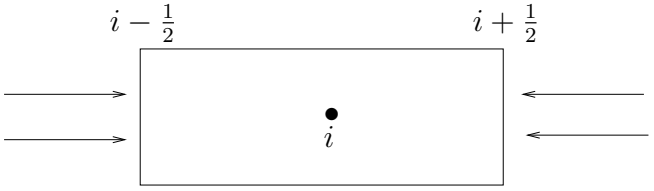

FIGURE 4.9: Flow of fluxes across discontinuity points in 1D

We assume that the properties of the medium are constant on each control volume. Simplifying the fluxes results in

$$-[A_{i+\frac{1}{2}} - A_{i-\frac{1}{2}} + B_{i+\frac{1}{2}} - B_{i-\frac{1}{2}}] = F_{v,T} \cdot dx$$

$\Longrightarrow$

$$A_{i-\frac{1}{2}} - A_{i+\frac{1}{2}} + B_{i-\frac{1}{2}} - B_{i+\frac{1}{2}} = F_{v,T} \cdot dx \tag{4.29}$$

Expanding, we have

$$
\begin{aligned}
&\lambda_T\left(S^n_{i-\frac{1}{2}}\right)\frac{\left(P^{n+1}_i-P^{n+1}_{i-1}\right)}{\triangle x_i}\\
&-\lambda_T\left(S^n_{i+\frac{1}{2}}\right)\frac{\left(P^{n+1}_{i+1}-P^{n+1}_i\right)}{\triangle x_i}\\
&+\frac{1}{2}\lambda_d\left(S^n_{i+\frac{1}{2}}\right)\left(P_c(S^n_{i+1})-P_c(S^n_i)\right)\\
&-\frac{1}{2}\lambda_d\left(S^n_{i-\frac{1}{2}}\right)\frac{\left(P_c(S^n_i)-P_c(S^n_{i-1})\right)}{\triangle x_i}=F_{v,T}\triangle x_i
\end{aligned}
\tag{4.30}
$$

Seeking P^{n+1}_{i+1} from the above equation (4.30), we have

$$
\begin{aligned}
P^{n+1}_{i+1}=P^{n+1}_i+\frac{1}{\lambda_T\left(S^n_{i+\frac{1}{2}}\right)}\Big[&\lambda_T\left(S^n_{i-\frac{1}{2}}\right)\left(P^{n+1}_i-P^{n+1}_{i-1}\right)\\
+\frac{1}{2}\lambda_d\left(S^n_{i-\frac{1}{2}}\right)&\left(P_c(S^n_i)-P_c(S^n_{i-1})\right)-\frac{1}{2}\lambda_d\left(S^n_{i+\frac{1}{2}}\right)\left(P_c(S^n_{i+1})-P_c(S^n_i)\right)\\
-F_{v,T}(i,n)&\triangle x_i^2\Big]
\end{aligned}
\tag{4.31}
$$

where we make use of the forward difference approximation of the derivatives.

Rearranging equation (4.31) gives

$$
-\lambda_T\left(S^n_{i-\frac{1}{2}}\right)P^{n+1}_{i-1}+\left[\lambda_T\left(S^n_{i-\frac{1}{2}}\right)+\lambda_T\left(S^n_{i+\frac{1}{2}}\right)\right]P^{n+1}_i-\lambda_T\left(S^n_{i+\frac{1}{2}}\right)P^{n+1}_{i+1}=b^{n+1}_i
\tag{4.32}
$$

where

$$
\begin{aligned}
b^{n+1}_i=&\frac{1}{2}\lambda_d\left(S^n_{i-\frac{1}{2}}\right)P_c(S^n_{i-1})+\frac{1}{2}\left[\lambda_d\left(S^n_{i-\frac{1}{2}}\right)+\lambda_d\left(S^n_{i+\frac{1}{2}}\right)\right]P_c(S^n_i)\\
&+\frac{1}{2}\lambda_d\left(S^n_{i+\frac{1}{2}}\right)P_c(S^n_{i+1})+F^{n+1}_{Ti}\triangle x_i^2
\end{aligned}
\tag{4.33}
$$

If we now let $a_m=\lambda_T\left(S^n_{i-\frac{1}{2}}\right)$ and $a_{i+1}=\lambda_T\left(S^n_{i+\frac{1}{2}}\right)$, then equation (4.33) can be written in the form of equation (4.19) as

$$
-a_mP^{n+1}_{m-1}+[a_m+a_{m+1}]P^{n+1}_m-a_{m+1}P^{n+1}_{m+1}=b^{n+1}_m
\tag{4.34}
$$

From equation (4.34), the systems of equations we get looks like

$$\begin{aligned}
-a_1P_0 + [a_1 + a_2]P_1 - a_2P_2 &= b_1 \\
-a_2P_1 + [a_2 + a_3]P_2 - a_3P_3 &= b_2 \\
&\dots \\
&\dots \\
&\dots \\
-a_{m-1}P_{m-2} + [a_{m-1} + a_m]P_{m-1} - a_mP_m &= b_{m-1} \\
-a_mP_{m-1} + [a_m + a_{m+1}]P_m - a_{m+1}P_{m+1} &= b_m
\end{aligned}$$

With Dirichlet boundary conditions, we require two boundary conditions $P(0) = P_0$ and $P(L) = P_L$ for the pressure. We note that it is the pressure difference between these two boundary conditions which actually drive the flow. Since this thesis makes use of only the cell centered grid, it implies, $P_{1/2} = P_0$ whilst $P_{n+1/2} = P_L$. In order to make the boundary conditions coincide with $P(0)$ and $P(L)$ respectively, we add ghost cells at the end of the interval and assume that the boundary conditions are specified at the ghost cells. Discretizing these ghost cells will lead us to get additional grid points x_0 and x_{n+1}. We then assume finally that $P_0 = P_0$ and $P_{n+1} = P_L$.

We move the boundary terms to the right hand side of the system of equations to give

$$\begin{aligned}
(a_1 + a_2)P_1 - a_2P_2 &= b_1 + a_1P_0 \\
-a_2P_1 + (a_2 + a_3)P_2 - a_3P_3 &= b_2 \\
&\dots \\
&\dots \\
&\dots \\
-a_{m-1}P_{m-2} + (a_{m-1} + a_m)P_{m-1} - a_mP_m &= b_{m-1} \\
-a_mP_{m-1} + (a_m + a_{m+1})P_m &= b_m + a_{m+1}P_L
\end{aligned}$$

Writing this in matrix form implies

$$A^{n+1} = \begin{pmatrix} a_1 + a_2 & -a_2 & 0 & . & . & . & 0 \\ -a_2 & a_2 + a_3 & -a_3 & . & . & . & . \\ 0 & -a_3 & a_3 + a_4 & -a_4 & . & . & . \\ 0 & \ddots & \ddots & \ddots & \ddots & \ddots & . \\ . & \ddots & \ddots & \ddots & \ddots & \ddots & . \\ . & & & \ddots & -a_{i-1} & a_{m-1} + a_m & a_m \\ 0 & & 0 & 0 & 0 & -a_m & a_m + a_{m+1} \end{pmatrix}.$$

and

$$b^{n+1} = \begin{pmatrix} b_1 + a_1 P_0 \\ b_2 \\ b_3 \\ . \\ . \\ b_{m-1} \\ b_m + a_{m+1} P_L \end{pmatrix}.$$

which gives the linear system

$$A\overline{P} = b$$

for

$$\overline{P} = [P_1, P_2, P_3, ..., P_{m-1}, P_m]^T$$

which can then be solved by the use of a numerical linear solver.

We note from figure 4.10

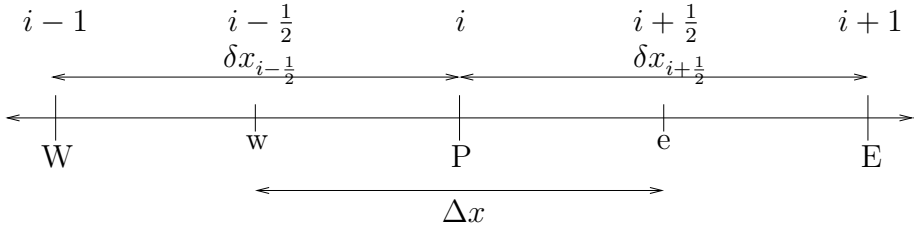

FIGURE 4.10: Standard nomenclature for control-volume discretization in 1D

that
$\lambda_T\left(S^n_{i+\frac{1}{2}}\right) = \frac{\lambda_T(S^n_{i+1})+\lambda_T(S^n_i)}{2}$
and
$\lambda_T\left(S^n_{i-\frac{1}{2}}\right) = \frac{\lambda_T(S^n_i)+\lambda_T(S^n_{i-1})}{2}$

In this thesis, the upwind approximation of mobilities is employed.

From the saturation equation in equation (3.16), we have

$$\frac{\phi\partial\left(S_w\right)}{\partial t} - \frac{d}{dx}\left[\lambda_w(S^n_w)\frac{d}{dx}\left(\overline{P}^{n+1} - \frac{1}{2}P_c(S^n_w)\right)\right] = \frac{F_{v,w}}{\rho_w} \tag{4.35}$$

Integrating equation (4.35) using the two point flux approximation results in

$$\phi\frac{S^{n+1}_i - S^n_i}{\triangle t} - \sum F = \frac{F_{v,w}}{\rho_w} \triangle x \tag{4.36}$$

where
$\sum F = F_1 + F_2 + F_3 + F_4$

with
$F_1 = -\lambda_w(S^n_{i-\frac{1}{2}}) \cdot \frac{dP}{dx}|_{i-\frac{1}{2}}$

$F_2 = -\frac{1}{2}\lambda_w(S^n_{i-\frac{1}{2}}) \cdot \frac{dP_c}{dx}|_{i-\frac{1}{2}}$

$F_3 = \frac{1}{2}\lambda_w(S^n_{i+\frac{1}{2}}) \cdot \frac{dP_c}{dx}|_{i+\frac{1}{2}}$

$F_4 = \lambda_w(S^n_{i+\frac{1}{2}}) \cdot \frac{dP}{dx}|_{i+\frac{1}{2}}$

Substituting for F_1 , F_2 , F_3 and F_4 into equation (4.36) and using the backward Euler discretization scheme for the time derivative gives,

$$\begin{aligned}\phi\frac{S^{n+1}_i - S^n_i}{\triangle t} + \lambda_w\left(S^n_{i-\frac{1}{2}}\right)\frac{dp}{dx} - \frac{1}{2}\lambda_w\left(S^n_{i-\frac{1}{2}}\right)\frac{dp_c(S^n_w)}{dx} \\ - \lambda_w\left(S^n_{i+\frac{1}{2}}\right)\frac{dp}{dx} + \frac{1}{2}\lambda_w\left(S^n_{i+\frac{1}{2}}\right)\frac{dp_c(S^n_w)}{dx} = \frac{F_{v,w}}{\rho_w}\triangle x_i.\end{aligned} \tag{4.37}$$

Seeking S^{n+1}_i from equation (4.37), we have

$$\begin{aligned}S^{n+1}_i = S^n_i + \frac{\triangle t}{\phi \triangle x^2}[\lambda_w(S^n_{i-\frac{1}{2}})(P^{n+1}_i - P^{n+1}_{i-1}) - \frac{1}{2}\lambda_w(S^n_{i-\frac{1}{2}})(P_c(S^n_i) - P_c(S^n_{i-1})) + \\ \lambda_w(S^n_{i+\frac{1}{2}})(P^{n+1}_{i+1} - P^{n+1}_i) - \frac{1}{2}\lambda_w(S^n_{i+\frac{1}{2}})(P_c(S^n_{i+1}) - P_c(S^n_i)) + \frac{F_{v,w}}{\rho_w}(\triangle x^2_i)].\end{aligned} \tag{4.38}$$

We note that, from the pressure equation (4.31) we first obtain P^{n+1}_{i+1} which we then use to find S^{n+1}_i, the saturation equation (4.38).

4.3.1 Discretization of the transport equation

We now discretize the conservative transport equation (3.21) in chapter 3 using the control volume method. Omitting the adsorption term and re-arranging results in

$$\frac{\partial(\theta C)}{\partial t} + \nu\frac{\partial C}{\partial x} - D\frac{\partial^2 C}{\partial x^2} - q_w = 0 \tag{4.39}$$

where $\theta = S_w\phi$ is the moisture content.

It is clear from the equation that C can be obtained explicitly. Integrating equation (4.39) on the standard nomenclature for control-volume methods figure 4.10 and applying the backward Euler discretization method for the time component, we have

$$\phi\int_{i-\frac{1}{2}}^{i+\frac{1}{2}} \frac{(S_{wi}^{n+1}C_i^{n+1}) - (S_{wi}^{n}C_i^{n})}{\Delta t}dx + \int_{i-\frac{1}{2}}^{i+\frac{1}{2}} \nu\frac{\partial C_i^n}{\partial x}dx - \int_{i-\frac{1}{2}}^{i+\frac{1}{2}} D\frac{\partial^2 C_i^n}{\partial x^2}dx - \int_{i-\frac{1}{2}}^{i+\frac{1}{2}} q_i^n dx = 0 \tag{4.40}$$

Now, S_w is already known from equation (4.38). This implies that equation (4.40) reduces to

$$\phi\int_{i-\frac{1}{2}}^{i+\frac{1}{2}} \frac{C_i^{n+1} - C_i^{n}}{\Delta t}dx + \int_{i-\frac{1}{2}}^{i+\frac{1}{2}} \nu\frac{\partial C_i^n}{\partial x}dx - \int_{i-\frac{1}{2}}^{i+\frac{1}{2}} D\frac{\partial^2 C_i^n}{\partial x^2}dx - \int_{i-\frac{1}{2}}^{i+\frac{1}{2}} q_i^n dx = 0 \tag{4.41}$$

This aspect of the thesis explains into details the discretization. We first consider the spatial components of equation (4.41) being

$$\int_{i-\frac{1}{2}}^{i+\frac{1}{2}} \nu\frac{dC_i^n}{dx}dx - \int_{i-\frac{1}{2}}^{i+\frac{1}{2}} D\frac{d^2 C_i^n}{dx^2}dx - \int_{i-\frac{1}{2}}^{i+\frac{1}{2}} q_i^n dx = 0 \tag{4.42}$$

Each term in this equation is evaluated and simplified separately using the central-difference finite volume model. The parts are then reassembled into a discrete equation relating C at node i to the C values at nodes $(i+1)$ and $(i-1)$.

4.3.2 The diffusion term

The second term in equation (4.42), being the diffusion term, shows the balance of transport by diffusion into the control volume . This integral can be evaluated exactly as

$$\int_{i-\frac{1}{2}}^{i+\frac{1}{2}} D\frac{d^2C_i^n}{dx^2}dx = \left(D\frac{dC}{dx}\right)_{i+\frac{1}{2}} - \left(D\frac{dC}{dx}\right)_{i-\frac{1}{2}} \tag{4.43}$$

Replacing the two diffusive fluxes by finite-difference approximations, we have

$$\left(D\frac{dC}{dx}\right)_{i+\frac{1}{2}} \approx D_{i+\frac{1}{2}}\frac{C_{i+1}^n - C_i^n}{\delta x_{i+\frac{1}{2}}} = \overline{D}_{i+\frac{1}{2}}(C_{i+1}^n - C_i^n)$$

$$\left(D\frac{dC}{dx}\right)_{i-\frac{1}{2}} \approx D_{i-\frac{1}{2}}\frac{C_i^n - C_{i-1}^n}{\delta x_{i-\frac{1}{2}}} = \overline{D}_{i-\frac{1}{2}}(C_i^n - C_{i-1}^n)$$

where $\overline{D}_{i+\frac{1}{2}} = \frac{D_{i+\frac{1}{2}}}{\delta x_{i+\frac{1}{2}}}$ and $\overline{D}_{i-\frac{1}{2}} = \frac{D_{i-\frac{1}{2}}}{\delta x_{i-\frac{1}{2}}}$

From figure 4.10, $\delta x_{i+\frac{1}{2}} = (i+1) - i$ and $\delta x_{i-\frac{1}{2}} = i - (i-1)$.

We bear in mind that C_i^n , C_{i+1}^n , and C_{i-1}^n are the values of C^n at the nodes i, $(i+1)$, and $(i-1)$ of figure 4.10. These are the discrete unknown that are obtained by solution of the finite volume model equations. Since this thesis considers only the case of uniform D, it implies $\overline{D}_{i+\frac{1}{2}} = \overline{D}_{i-\frac{1}{2}} = \overline{D}$. Equation (4.43) now becomes

$$\int_{i-\frac{1}{2}}^{i+\frac{1}{2}} D\frac{d^2C_i^n}{dx^2}dx = \overline{D}_{i+\frac{1}{2}}(C_{i+1}^n - C_i^n) - \overline{D}_{i-\frac{1}{2}}(C_i^n - C_{i-1}^n) \tag{4.44}$$

4.3.3 The source term

The discrete contribution of the source term is obtained by assuming that $(q^n + R(C^n))$ has the uniform value of $(q^n)_i$ throughout the control volume. Thus,

$$\int_{i-\frac{1}{2}}^{i+\frac{1}{2}} q^n dx \approx q_i^n \Delta x \tag{4.45}$$

The distribution of $q_i^n \Delta x$ will be supplied as an input to the model.

4.3.4 The convection term

The convective term in equation (4.42) can be integrated once exactly as

$$\int_{i-\frac{1}{2}}^{i+\frac{1}{2}} \nu \frac{dC_i^n}{dx} dx = (\nu C^n)_{i+\frac{1}{2}} - (\nu C^n)_{i-\frac{1}{2}} \tag{4.46}$$

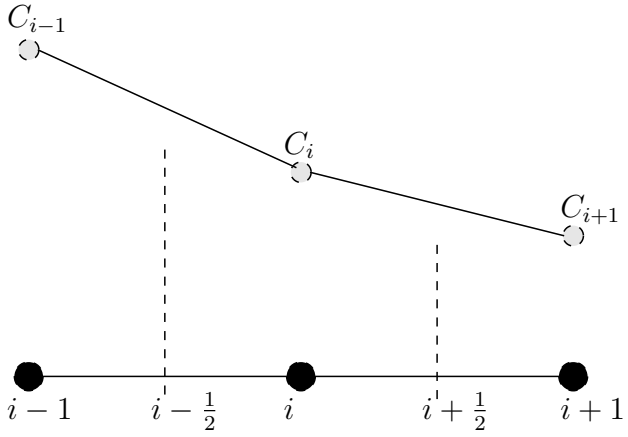

FIGURE 4.11: Linear interpolation to obtain interface values $C^n_{i-\frac{1}{2}}$ and $C^n_{i+\frac{1}{2}}$ for the central difference approximation

.

In evaluating the right hand side of the above expression, the values of $C^n_{i+\frac{1}{2}}$ and $C^n_{i-\frac{1}{2}}$ need to be estimated. In the finite volume method, the values of C_i^n are stored only at the nodes i, $(i+1)$, and $(i-1)$. The method for determining an interface value such as $C^n_{i+\frac{1}{2}}$ from the nodal values such as C_i^n and C_{i+1}^n has important consequences for the accuracy of the numerical model. Various methods exist for estimating $C^n_{i+\frac{1}{2}}$ in terms of the nodal values C_{i+1}^n and C_i^n. In this thesis, the common linear interpolation method as depicted in figure 4.11 is used. The linear interpolation formula can be written as:

$$C^n_{i+\frac{1}{2}} = \beta_{i+\frac{1}{2}} C^n_{i+1} + (1 - \beta_{i+\frac{1}{2}}) C^n_i \tag{4.47}$$

in which

$$\beta_{i+\frac{1}{2}} = \frac{\left(i+\frac{1}{2}\right) - i}{(i+1) - i} \tag{4.48}$$

Thus, equations (4.48) and (4.47) constitutes the central difference scheme for approximating the derivatives

$$\frac{d(\nu C^n)}{dx}\,|_{i+\frac{1}{2}} \approx \frac{(\nu C^n)_{i+1} - (\nu C^n)_i}{(i+1) - i}$$

Again, using linear interpolation to estimate $C^n_{i-\frac{1}{2}}$ in terms of C^n_{i-1} and C^n_i gives

$$C^n_{i-\frac{1}{2}} = \beta_{i-\frac{1}{2}} C^n_{i-1} + (1 - \beta_{i-\frac{1}{2}}) C^n_i \tag{4.49}$$

where

$$\beta_{i-\frac{1}{2}} = \frac{i - \left(i - \frac{1}{2}\right)}{i - (i-1)} \tag{4.50}$$

Since this thesis is limited to only uniform mesh and also due to the fact that the nodes are located midway between the cell faces, it implies $\beta_{i-\frac{1}{2}} = \beta_{i+\frac{1}{2}} = \frac{1}{2}$. We now substitute equations (4.47) and (4.49) into (4.46) and rearranging, results in

$$\int_{i-\frac{1}{2}}^{i+\frac{1}{2}} \nu \frac{dC^n_i}{dx} dx = \nu_{i+\frac{1}{2}} \beta_{i+\frac{1}{2}} (C^n_{i+1} - C^n_i) - \nu_{i-\frac{1}{2}} \beta_{i-\frac{1}{2}} (C^n_{i-1} - C^n_i) + \nu_{i+\frac{1}{2}} C^n_i - \nu_{i-\frac{1}{2}} C^n_i \tag{4.51}$$

Since ν is a uniform parameter, we have $\nu_{i+\frac{1}{2}} = \nu_{i-\frac{1}{2}} = \nu$. Hence the last two terms in the preceding equation cancels. This reduces equation (4.51) to

$$\int_{i-\frac{1}{2}}^{i+\frac{1}{2}} \nu \frac{dC^n_i}{dx} dx = \nu \beta_{i+\frac{1}{2}} (C^n_{i+1} - C^n_i) - \nu \beta_{i-\frac{1}{2}} (C^n_{i-1} - C^n_i) \tag{4.52}$$

If we now substitute equations (4.44) , (4.45) and (4.52) into equation (4.42) and simplify, it results in the discrete form of the spatial components. This gives

$$-a_{i+1} C^n_{i+1} + a_i C^n_i - a_{i-1} C^n_{i-1} = b^n_i \tag{4.53}$$

where

$$a_{i+1} = \frac{1}{\Delta x} (\overline{D}_{i+\frac{1}{2}} - \nu \beta_{i+\frac{1}{2}}) \tag{4.54}$$

$$a_{i-1} = \frac{1}{\Delta x}(\overline{D}_{i-\frac{1}{2}} - \nu\beta_{i-\frac{1}{2}}) \tag{4.55}$$

$$a_i = a_{i+1} + a_{i-1} \tag{4.56}$$

$$b_i^n = q_i^n \tag{4.57}$$

For the discretization of the time component in (4.41), we have

$$\phi \int_{i-\frac{1}{2}}^{i+\frac{1}{2}} \frac{C_i^{n+1} - C_i^n}{\Delta t} dx = \phi \left(\frac{C_i^{n+1} - C_i^n}{\Delta t} \right) \Delta x \tag{4.58}$$

which is considered to be a constant averaging of the concentration C_i^n on each cell.

We now add equation (4.58) and (4.53) to give us the fully discretized equation for our transport model (4.39). Hence, for our discretized transport model, we have

$$\phi \left(\frac{C_i^{n+1} - C_i^n}{\Delta t} \right) \Delta x - a_{i+1} C_{i+1}^n + a_i C_i^n - a_{i-1} C_{i-1}^n = b_i^n \tag{4.59}$$

Rearranging equation (4.59), C_i^{n+1} can be derived explicitly from the equation

$$C_i^{n+1} = C_i^n + \frac{\Delta t}{\phi \Delta x} \left[a_{i+1} C_{i+1}^n - a_i C_i^n + a_{i-1} C_{i-1}^n + b_i^n \right] \tag{4.60}$$

Chapter 5

Numerical results and analysis

The numerical results of the simulations are presented in this chapter and they are based on the discretization discussed in chapter 4. In order to test the accuracy of the model, we run our model on some simulations problem designed in an article published by Brahim Amaziane, Mladen Jurak and Ana Keko [27]. Their work focused on modeling and simulations of immiscible compressible two-phase flow in porous media by the concept of global pressure. Their model was tested with the Couplex-Gas benchmark (2006) which has currently been proposed to improve the simulation of the migration of hydrogen produced by the corrosion of nuclear waste packages in an underground storage. The results of their simulations are presented for the differences in phase pressures and water saturation.

5.1 Model validation with the couplex-gas benchmark

For the numerical analysis, a set of data was taken from the couplex-Gas benchmark with incompressible wetting phase (water) and the ideal gas law $\rho_g(p_g) = c_g p_g$ for the nonwetting phase (hydrogen) and a set of van Genuchten's parameters. The fluid properties and other parameters used are given in table 5.1 below, in which n and entry pressure P_e are the van Genuchten's parameters.

Parameter	Values
K	1 mD
ϕ	0.1
n	2
L	100 m
P_e	2 MPa
ρ_w	996.5 kg/m^3
ρ_o	2 kg/m^3
μ_w	0.869 x 10^{-3} $Pa\ s$
μ_g	9 x 10^{-6} $Pa\ s$

TABLE 5.1: Benchmark fluid properties and other parameters

The van Genuchten's capillary pressure and relative permeabilities are given by the relations:

$$P_c(S_w) = P_e\left(\left(S_w^{-1/m} - 1\right)^{1/n}\right),$$
$$K_{rw}(S_w) = \sqrt{S_w}\left[\left(1 - \left(1 - S_w^{1/m}\right)^m\right)\right]^2$$
$$K_{ro}(S_w) = \sqrt{1 - S_w}\left[\left(1 - S_w^{1/m}\right)^{2m}\right]$$

In the above formulas, we have $m = 1 - 1/n$ and assume that water and gas residual saturations are equal to zero. Figure 5.1 shows how they look.

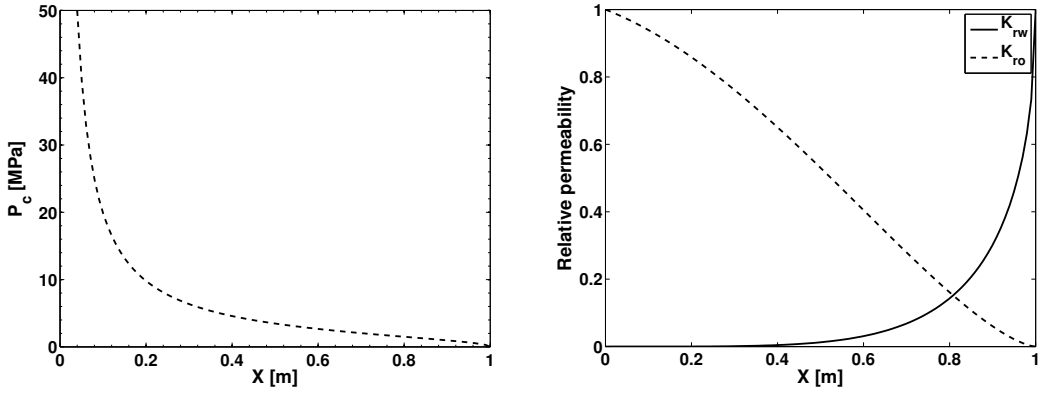

(a) Capillary pressure

(b) Relative permeabilities

FIGURE 5.1: van Genuchten's parameters

Three different simulations corresponding to gas injection, imbibition and gas source terms were presented in this papers. This thesis showcases just two of them.

5.1.1 Benchmark simulation one

In this simulation, the gas is injected on the left end of the porous medium initially saturated with water. As in other simulations, they use Dirichlet boundary conditions for the global pressure and a Dirichlet boundary condition for the water saturation on injection boundary completed by the Neumann condition on the output end of the domain. Their governing equations were solved using the following boundary conditions:

$$S_w(0,4) = 0.4, \quad p(0,t) = 2.0, \quad p(L,t) = 0.1, \quad \frac{\partial}{\partial x} S_w(L,t) = 0$$

and initial conditions:

$$S_w(x,0) = 1.0, \quad p(x,0) = 0.1.$$

The source terms are equal to zero. Thus $F_w = F_g = 0$. With the assumptions that our nonwetting phase is gas, we solved our governing equation (3.16) with the same boundary conditions. We defined their global pressure in terms of our water pressure using equation (3.13) and specify boundary conditions for the water phase pressure. This yielded the following boundary conditions:

$$S_w(0,4) = 0.4, \quad p_w(0,t) = 4.09 - P_c(0.4)/2, \quad p_w(L,t) = 0.1, \quad \frac{\partial}{\partial x} S_w(L,t) = 0.$$

and initial conditions:

$$S_w(x,0) = 1.0, \quad p_w(x,0) = 0.1.$$

The same fluid properties were ascribed to the oil and the simulation time T is 45 days. The results of simulations one are found in figure 5.2. The results are in correspondence with the ones in [27], please see Fig. 5 in [27].

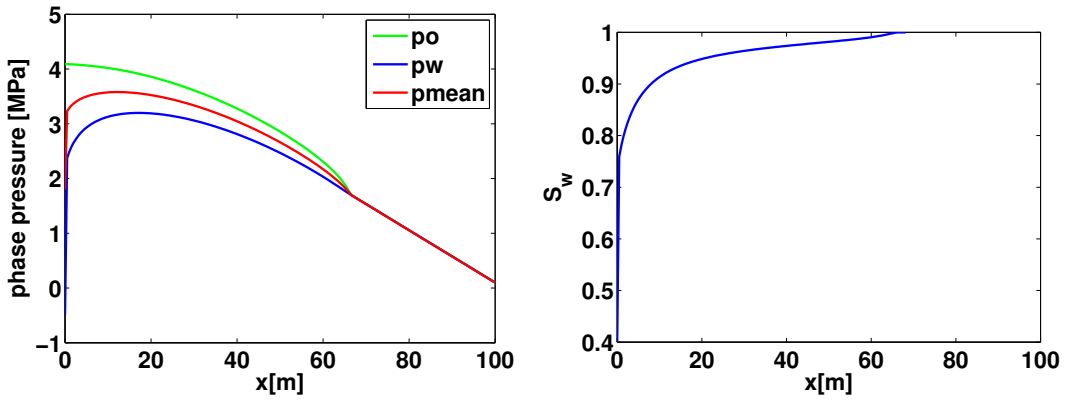

(a) Pressure phases

(b) Saturation

FIGURE 5.2: Benchmark simulation one. Pressure and water saturation profiles at time T = 45 days.

5.1.2 Benchmark simulation two

Simulation two concerns an imbibition process in which pure water is injected in the porous domain filled with 30% of gas. Their governing equations were solved using the following boundary conditions:

$$S_w(0,4) = 1.0, \quad p(0,t) = 4.0, \quad p(L,t) = 0.5, \quad \frac{\partial}{\partial x} S_w(L,t) = 0$$

and initial conditions:

$$S_w(x,0) = 0.7, \quad p(x,0) = 0.5$$

whilst ours was solved using

$$S_w(0,4) = 1.0, \quad p_w(0,t) = 4.0, \quad p_w(L,t) = 2.3 - P_c(0.7)/2, \quad \frac{\partial}{\partial x} S_w(L,t) = 0$$

and initial conditions:

$$S_w(x,0) = 1.0, \quad p_w(x,0) = 2.3 - P_c(0.7)/2.$$

Again, the source terms are zero. Thus $F_w = F_g = 0$.

The above simulation two yielded the following results in figure 5.3 which are consistent with Fig. 6 Simulation 2 in [27].

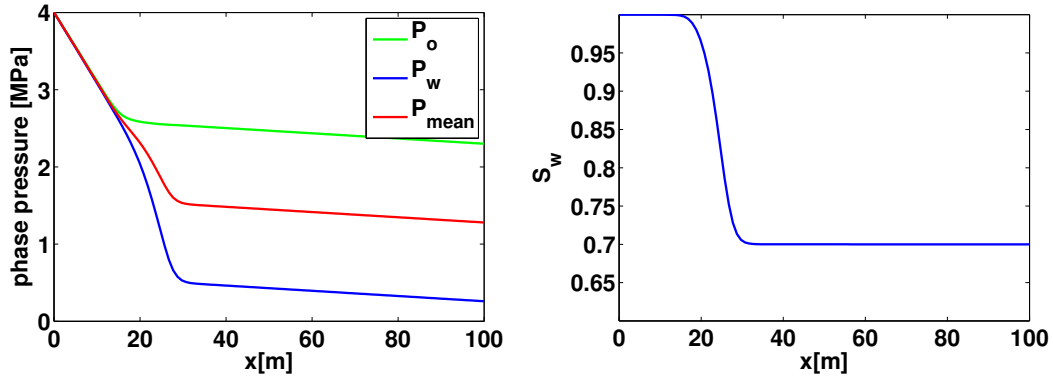

(a) Pressure phases

(b) Saturation

FIGURE 5.3: Benchmark simulation two. Pressure and water saturation profiles at time T = 45 days.

The results of both simulations are very much consistent with the physics. We see in simulation one that a higher pressure was imposed at the injection boundary so as to be able to drive the less dense phase being gas into the much denser phase being water. Only small regions of the domain is occupied by the gas and the remaining part of the domain is fully saturated with water causing all pressures to coincide after over 60 meters into the domain. This must be so because capillary effect is absent at regions which are fully saturated with one phase. In simulation two, after 45 days, 20 meters into the domain is fully saturated with water. This caused the phase pressures to coincide 20 meters into the domain. Both results are trivial in that it is much easier for a less dense fluid to be displaced by a high dense fluid.

The results from both simulations are enough to attest to the fact that our model problem equation (3.16) can be trusted for further simulations. We again prove this point by constructing an analytical solution for the mean pressure and water saturation and show some convergence analysis.

5.2 Model validation with an analytical solution

The main aim of this section is to show some convergence analysis for our model. As spelled out in the article of Radu et. al. [19], we first construct an analytical solution which fits the system and perform several numerical simulations with different sizes of the time and space step. Secondly, we compare our numerical solutions with the constructed analytical solutions by comparing the errors in the 2-norm and the L^{∞}-norm. A constructed numerical solution only implies that we choose a simple solution which we know satisfies the initial and boundary conditions and then we adjust the equations such that the analytical solutions will be the exact solutions of the set of equations. This procedure is quite common when comparing an analytical solution with its' numerical solution.

5.2.1 The set of equations and the parameters used

We now solve numerically our equation (3.16) within a dimensionless domains of time $t \, \epsilon \, [0, T]$ and space $x \, \epsilon \, [0, L]$. With regards to parameters to describe the capillary pressure and the relative permeabilities, the Brooks-Corey parameters of the type;

$$\begin{cases} P_c(S_w) = S_w^{-\frac{1}{\lambda}} \\ K_{rw}(S_w) = S_w^M \\ K_{ro}(S_w) = (1 - S_w)^2(1 - S_w)^N \end{cases}$$

with $\lambda = 2$, being the pore size distribution index which ranges between $0.2 \leq \lambda \leq 3$, $N = \frac{2}{\lambda} + 1$ and $M = N + 2$ is used.

We then construct an analytical solutions for $\widetilde{\overline{P}}$ and $\widetilde{S}_w$. These equations will then super impose initial and boundary conditions for our numerical solution.

$$\widetilde{S}_w(x, t) = 0.2 + 0.8xt, \quad S_w \, \epsilon \, [0, 1] \tag{5.1}$$

$$\widetilde{\overline{P}}(x, t) = xt(1 - x) + 2t. \tag{5.2}$$

We now use our analytical solutions to find the respective sources and sink terms for our mean pressure and water saturation. For simplicity, we let $P_c = P^{cap}$,

$S_w = S$, $F_{v,T} = F^T$, $F_{v,w} = F^w$, $\lambda_T = \lambda^T$, $\lambda_d = \lambda^d$, $\mu_o = \mu^o$, $\mu_w = \mu^w$ and $\rho_w = \rho^w$
Then equation (3.16) in one dimension gives

$$-\left(\lambda^T(S)\overline{P}_x + \tfrac{1}{2}\lambda^d(S)(P^{cap}(S))_x\right)_x = F^T$$
$$\phi S_t - \left(\left(\lambda^w(S)\overline{P}_x - \tfrac{1}{2}\lambda^w(S)(P^{cap}(S))_x\right)_x = \tfrac{F^w}{\rho^w}\right.$$

$\Longrightarrow$

$$-\left[(\lambda^T(S)_x\overline{P}_x + \lambda^T(S)\overline{P}_{xx} + \frac{1}{2}(\lambda^d(S)_x(P^{cap}(S))_x + \lambda^d(S)(P^{cap}(S))_{xx})\right] = F^T \tag{5.3}$$

and

$$\phi S_t - \left[(\lambda^w(S))_S S_x\overline{P}_x + \lambda^w(S)\overline{P}_{xx} - \left(\frac{1}{2}(\lambda^w(S))_S S_x(P^{cap}(S))_{xx}\right)\right] = \frac{F^w}{\rho^w} \tag{5.4}$$

Now from the brooks-Corey parameters, we have

$$(\lambda^T(S))_S = \frac{mS^{m-1}}{\mu^w} - \frac{2(1-S)(1-S^n) + n(1-S)^2S^{n-1}}{\mu^o} \tag{5.5}$$

$$(\lambda^d(S))_S = -\left[\frac{2(1-S)(1-S^n) + n(1-S)^2S^{n-1}}{\mu^o} + \frac{mS^{m-1}}{\mu^w}\right] \tag{5.6}$$

$$(P^{cap}(S))_S = -\frac{S^{-\left(\frac{1}{\lambda}+1\right)}}{\lambda} \tag{5.7}$$

$$((P^{cap}(S))_{SS} = \frac{(1+\lambda)}{\lambda}S^{-(\frac{1}{\lambda}+2)} \tag{5.8}$$

where

$$\lambda^T(S) = \frac{S^m}{\mu^w} + \frac{(1-S)^2(1-S^n)}{\mu^o}$$

$$\lambda^d(S) = \frac{(1-S)^2(1-S^n)}{\mu^o} - \frac{S^m}{\mu^w}$$

If we now differentiate (5.5) to (5.8) with respect to x, taking note of the chain rule and substituting the terms respectively into equations (5.3) and (5.4); simplifying gives

$$\widetilde{F^w} = \rho^w \left[\phi S_t - \frac{mS^{m-1}}{\mu^w} S_x P_x + P_{xx} \frac{S^m}{\mu^w} - \frac{mS^{m-1}}{2\mu^w} (S_x)^2 \left(\frac{1}{\lambda} S^{-(\frac{1}{\lambda}+1)} \right) + \frac{1}{2} \frac{S^m}{\mu^w} \left(\frac{1+\lambda}{\lambda^2} S^{-(\frac{1}{\lambda}+2)} \right) S_x \right] \tag{5.9}$$

and

$$\widetilde{F^T} = (\lambda^T(S))_S S_x P_x + \lambda^T(S) P_{xx} + \frac{1}{2} (\lambda^d(S))_S (S_x)^2 \left(\frac{1}{\lambda} S^{-(\frac{1}{\lambda}+1)} \right) - \frac{1}{2} \lambda^d(S) \left(\frac{1+\lambda}{\lambda^2} S^{-(\frac{1}{\lambda}+2)} \right) S_x \tag{5.10}$$

in which we have from (5.1) and (5.2)

$$\widetilde{\overline{P}}_x = t - 2\ x\ t \tag{5.11}$$

$$\widetilde{\overline{P}}_{xx} = -2t \tag{5.12}$$

$$(\widetilde{S})_x = 0.8t \tag{5.13}$$

$$(\widetilde{S})_{xx} = 0 \tag{5.14}$$

$$(\widetilde{S})_t = 0.8x \tag{5.15}$$

5.2.2 Comparison of results

To compare the numerical solution with the analytical one, we require some form of measure for the difference between them, in the form of a norm. From Florin Radus' lecture notes on numerical analysis [20], we will make use of both the L^2-norm and L^∞-norm which are defined as

$$||u||_2 = \left(\int |u| dx \right)^{\frac{1}{2}}$$

and

$$||u||_\infty = \max_{x \to [0,1]} |u|$$

for a function u. We will then compute the error for $\overline{P}$ and S_w as

$$E = ||u_{anal}(x,T) - u_{num}(x,T)||_2$$

where $u_{anal}(x,T)$ and $u_{num}(x,T)$ denote the analytical and numerical solutions respectively at $t = T$, being the final time. In this test, we let $t \epsilon [0,1]$, making $T = 1$. The squared error is then given by

$$E^2 = ||u_{anal}(x,T) - u_{num}(x,T)||_2^2 = \int_0^1 |u_{anal}(x,T) - u_{num}(x,T)|^2 dx,$$

from $x \epsilon [0,1]$. We recall that when we solve the equations numerically, we do divide the interval [0,L] into subintervals which we call cells with the midpoints $x_1, x_2, ..., x_n$, and integrate over each cell as seen in chapter 4. A similar thing is done here where we arrive at

$$E^2 = \sum_{i=1}^{n} \int_{x_{i-\frac{1}{2}}}^{x_{i+\frac{1}{2}}} |u_{anal}(x,T) - u_{num}(x,T)|^2 dx,$$

A simple percentage error analysis was made for the 2-norm and the ∞-norm respectively and the results shown in tables 5.2 and 5.3.

t	h	**% 2-norm**	**Reduction**	**% ∞-norm**	**Reduction**	Convergence rate (α)
0.2	0.2	9.0877	-	13.3333	-	
0.1	0.1	4.8353	1.8794490518	7.2727	1.833335625	0.9103
0.05	0.05	2.4956	1.9375300529	3.8095	1.9090956818	0.9542
0.025	0.025	1.2543	1.9896356534	1.9512	1.9523882739	0.9925
0.0125	0.0125	0.62668	2.0014999681	0.98765	1.9755986432	1.0011

TABLE 5.2: Error analysis for saturation

t(day)	**h(m)**	**% 2-norm**	**Reduction**	**% ∞-norm**	**Reduction**	Convergence rate (α)
0.2	0.2	2.757	-	6.4231	-	
0.1	0.1	1.7341	1.5898737097	3.9349	1.6323413556	0.6689
0.05	0.05	0.93812	1.8484842024	2.1078	1.8668279723	0.8863
0.025	0.025	0.48041	1.9527486938	1.0808	1.9502220577	0.9655
0.0125	0.0125	0.23699	2.0271319465	0.50733	2.1303687935	1.0194

TABLE 5.3: Error analysis for pressure

Figure 5.4 below shows the error plot. It is candid from the figure that as the time step decreases, the errors become smaller and converge. The convergence is of order 2 as seen from the error reduction columns in table 5.2 and 5.3 respectively.

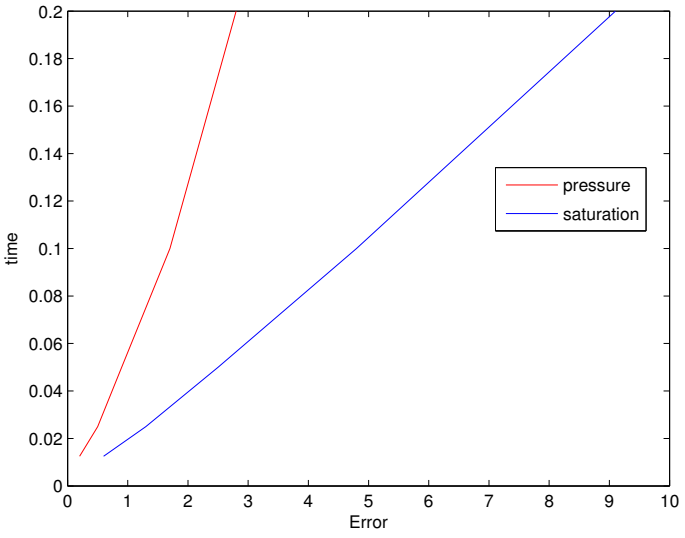

FIGURE 5.4: Error plots for pressure and saturation

Theoretically, we know that

$$E^2 = ||u_{anal}(x,T) - u_{num}(x,T)||_2^2$$

But

$$E^2 = \kappa^2(\triangle t)^{2p}$$

where p is the convergence rate and κ, a constant.

$\Longrightarrow$

$$E_i^2 = \kappa^2(\triangle t)^{2p}$$

$$E_{i+1}^2 = \kappa^2\left(\frac{\triangle t}{2}\right)^{2p}$$

$\Longrightarrow$

$$\left(\frac{E_i}{E_{i+1}}\right)^2 = \frac{\kappa^2(\triangle t)^{2p}}{\kappa^2\left(\frac{\triangle t}{2}\right)^{2p}}$$

Hence, we have the rate of convergence p given by

$$p = \log_2\left(\frac{E_i}{E_{i+1}}\right)$$

The last columns of tables 5.2 and 5.3 reveal that the model has a linear rate of convergence. It is clear from the tables that our model converges.

Chapter 6

Modeling of MEOR activities

6.1 A case study

Based on our benchmark in chapter 5, we carefully formulated a base case study on which we simulate the activities of microbial to see their effects on the model. We considered a case in which a reservoir of length $L = 100m$ having an initial oil saturation of 30%. An imbibition process was performed by first injecting water into the left side of the porous domain. For the numerical test of this case, a set of data was taken from a paper published by Sidsel M. Nielsen on 1D Simulation for Microbial Enhanced Oil Recovery with Metabolite Partitioning [28]. Table 6.1 summarizes the fluid properties and other parameters used for this case study and other simulations. We again employed van Genuchten's correlation functions with the same assumptions that the water and oil residual saturations are equal to zero. In this simulation, we specify Dirichlet boundary conditions for the water pressure and the Dirichlet condition for water saturation on injection boundary completed by a Dirichlet condition on the output end of the domain. Thus, we solve our governing equation (3.16) using the following boundary conditions:

$$S_w(0,t) = 1, \quad p(0,t) = 40.0, \quad p(L,t) = 1 - P_c(0.7)/2, \quad S_w(L,t) = 0.7$$

and initial conditions:

$$S_w(x,0) = 0.7, \quad p(x,0) = 1 - P_c(0.7)/2$$

The source terms are equal to zero. Thus $F_w = F_o = 0$. This implies that we have imposed a very high water injection pressure and lowered it at the output boundary. The results of this simulation are shown in figure 6.1 for the time instance of 45 days. We notice from the figure below that water saturation is one only on the boundary. This demands that both phase pressures must start at the same point on the boundary just as seen.

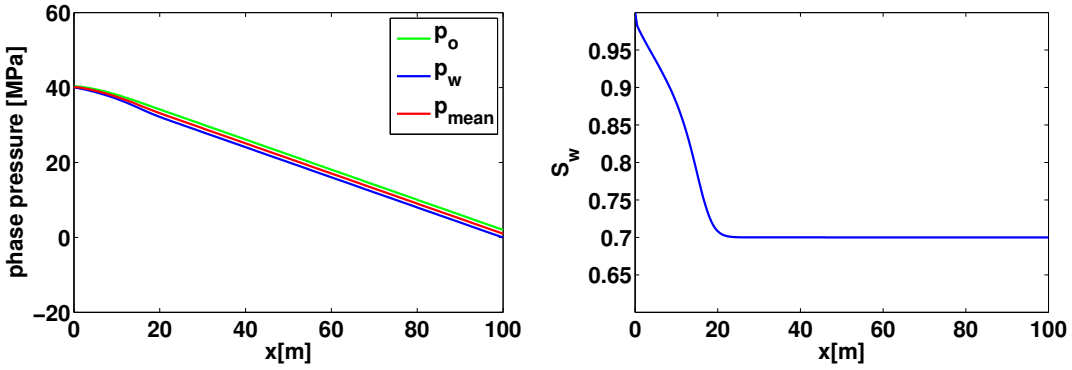

(a) Pressure phases

(b) Saturation

FIGURE 6.1: A case study. Pressure and water saturation profiles at time T = 45 days.

6.2 Effects of introducing microbial into the model

This section focuses on how we incorporate microbial models into the two-phase flow model for enhancement of the oil recovery. Most of the concepts employed in this section are basically the same as in the papers by Islam (1990) [29] and Nielsen et al. [28]. As seen in table 2.1 of chapter 2, enhancement of the oil recovery through microbial action can be performed through several mechanisms such as;

- Reduction of oil-water inter-facial tension and alteration of wettability by surfactant production and bacterial presence.
- Selective plugging by bacteria and their metabolites.
- Viscosity reduction by gas production or degradation of long-chain saturated hydrocarbons.
- Generation of acids that dissolve rock improving absolute permeability.

Out of these four mechanisms, the first two are believed to have the greatest impact on recovery, see please (Jenneman et al., 1984 and Bryant et al., 1989.)
Islam (1990) came out with a mathematical model for MEOR describing growth which leads to plugging, reduction of viscosity and inter-facial tension and the production of gas. Thus, he investigated four different mechanisms by which bacteria helps in recovery of the residual oil. This research investigated two of the mechanism presented by Islam (1990).

Bacteria produce surfactants by consumption of substrates. Surfactant decreases oil/water inter-facial tension and can be distributed between both phases. Several methods are used to model relative permeability changes as a function of inter-facial tension. A correlation between surfactant concentration and inter-facial tension σ was employed. Actually, a reduction of inter-facial tension decreases residual oil saturation and straightens the relative permeability curves approaching full miscibility (Coats, 1980; Al-Wahaibi et al., 2006).

The two mechanisms investigated in the paper are:

- Inter-facial tension-reducing surfactant generation

- Oil viscosity-reducing surfactant generation

Based on the model described in [28], we modify our reactive transport model equation (3.21) to describe convection-diffusion, bacterial growth and metabolite production, where metabolite is surfactant. Thus, our water phase now consist of water, bacteria and metabolite. The oil phase consists primarily of oil, but contains also metabolite. Figure 6.2 illustrates components and phases of the flow system. Surfactant can lower the oil/water inter-facial tension that has an effect on relative permeability curves. We assume the following for our model:

• Bacterial growth rate can be described by Monod kinetics being independent of temperature, pressure, pH and salinity.
• Metabolite is surfactant and can be distributed between both phases according to a distribution constant K_i and masses of water and oil.
• Neglecting adsorption of bacterial and thus plugging porous medium by bacteria.
• No substrate and metabolite adsorption to pore walls.
• Negligible chemotaxis.
• Isothermal system with incompressible flow.
• No volume change on mixing.

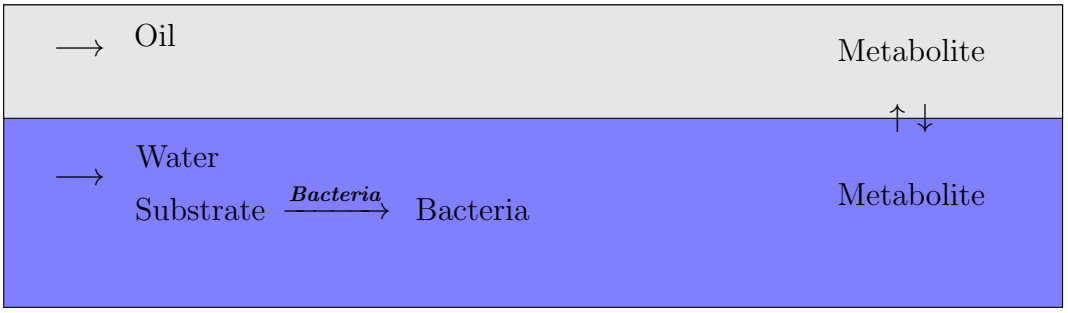

FIGURE 6.2: An oil reservoir

6.2.1 Inter-facial tension reduction with bacteria concentration

In modeling bacteria-generated surfactant flood, it is assumed that inter-facial tension is a function of bacteria concentration. In many cases, the relationship between these two parameters looks like figure 6.3. This figure has been extrapolated from data taken from the graph. Water-flooded systems have inter-facial

tensions between oil and water that are around $(20 - 30mN/m)$. In order to increase recovery significantly, a good surfactant should decrease inter-facial tension three or four orders of magnitude (Fulcher et al., 1985; Shen et al., 2006).

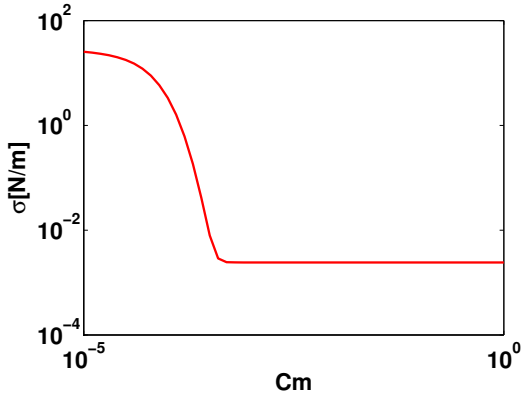

FIGURE 6.3: Inter-facial tension correlation with bacteria concentration

We also make use of the correlation between inter-facial tension and relative permeability curves as given in Islam (1990). They followed the work by Bang and Caudle [30] who predicted that the curves were related to inter-facial tension in the following manner:

$$K_{ro} = K_{ro}(S_o) + (S_o - K_{ro}) \left[\frac{\sigma_{max} - \sigma(C_b)}{\sigma_{max}} \right]$$

$$K_{rw} = K_{rw}(S_w) + (S_w - K_{rw}) \left[\frac{\sigma_{max} - \sigma(C_b)}{\sigma_{max}} \right]$$

This formulation assumes that the relative permeabilities to water and oil are straight lines extending from zero to one. Thus, in the limit as $\sigma \to 0$, these relative permeability curves approaches straight line forms. The van Genuchten's relative permeability curves will also be used and a comparison analysis will be made for the water saturations and their corresponding fractions of oil left in the reservoir per time. Also, the following capillary pressure curve was used in order to incorporate dependence of the capillary pressure on $\sigma(C_b)$. As specified in [31] which is used by the popular Eclipse simulator we have

$$p_c(\sigma(C_b), S_w) = P_e P_c(S_w) \left[\frac{\sigma(C_b)}{\sigma_{max}} \right] \tag{6.1}$$

where p_c becomes 0 if σ is 0.

Initial reservoir conditions for this simulation are found in table 6.1 at the end of this chapter. We compare our results with the base case study. We inject a mixture of bacteria together with substrate into the reservoir after water flooding and we compare results for the case of van Genuchten and Brooks-Corey parameters. The result of this simulations are found in figures 6.4 and 6.6 respectively.

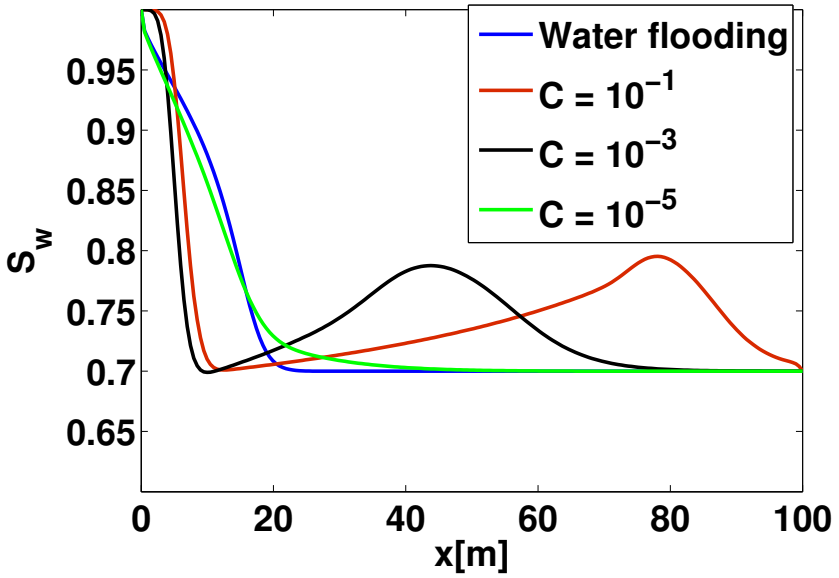

FIGURE 6.4: Saturation profile for van Genuchten parameter with different concentrations

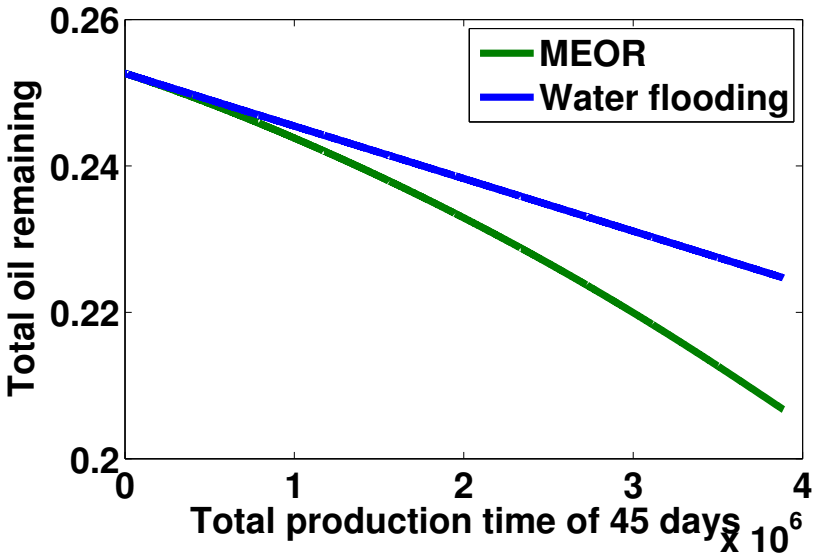

FIGURE 6.5: Fraction of oil remaining in the reservoire after 45 days using van Genuchten parameters with focus on inter-facial tension reduction

With a simulation time of just 45 days, the total oil left in the reservoir with the case of water flooding ($C = 0kg/m^3$) and ($C = 10^{-5}kg/m^3$) gave a mass of 22.56% and 22.51% respectively. As we increase the concentration of the bacteria together with substrates ($C = 10^{-3}kg/m^3$), the remaining mass of oil left is 21.72%. Finally with a high concentration of ($C = 10^{-1}kg/m^3$), the remaining mass of oil left is 20.79%. We note here that any further increase in bacteria concentration beyond ($C = 10^{-1}kg/m^3$) does no longer have much significant effect on the Inter-facial tension since it approaches the minimum. See figure 6.4. It is trivial to note that, both the case of water flooding and that of ($C = 10^{-5}kg/m^3$) gave quite close percentages of mass recovered. This is expected since bacteria concentration has to increase substantially away from the injection well so as to mobilize oil near the production well bore. However, as the concentration of the bacteria increases oil production increases. As the production time increases, more oil will be mobilized with the case of bacteria than that of water flooding because bacteria will grow and degrade more hydrocarbons which will in turn create an oil bank which will increase the recovery factor. Figure 6.5 displays the fraction of oil left in the reservoir for a highly concentrated MEOR flooding as against water flooding.

With the same simulation time of 45 days, similar arguments as in the case of van Genuchten's parameters hold. But comparatively, van Genuchten's parameters had a better significant recovery than Brooks-Corey parameters. This can be seen

in the two figures. A simple reason could be due to the choice of the parameter λ being used. In this thesis, we choose $\lambda = 2$ which is commonly used. With regards to MEOR modeling, various parameters ought to be experimented in order to find a best fit for effective recovery. The total oil remaining in the reservoir with the case of water flooding ($C = 0kg/m^3$) and ($C = 10^{-5}kg/m^3$) is 24.93% and 24.87% respectively. As we increase the concentration of bacteria to ($C = 10^{-3}kg/m^3$), the remaining mass of oil left is 24.63%. Finally with a high concentration of ($C = 10^{-1}kg/m^3$), the remaining mass of oil left is 24.42%. Indeed with our choice of λ, the Brooks-Corey's parameters has performed poorly against the van Genuchten's parameters. See figure 6.7 which displays the fraction of oil left in the reservoir for a highly concentrated MEOR flooding as against water flooding using Brooks Corey's parameters.

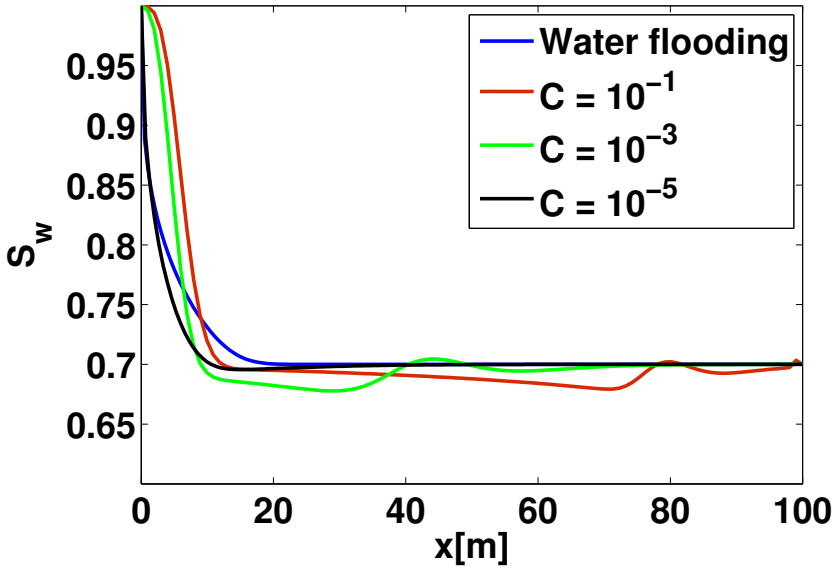

FIGURE 6.6: Saturation profile for Brooks Corey parameter with different concentrations

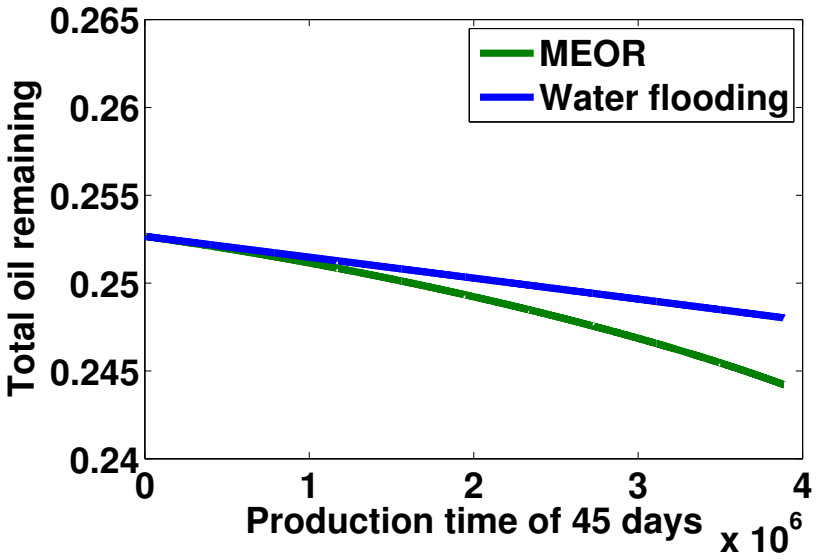

FIGURE 6.7: Fraction of oil remaining in the reservoire after 45 days using Brooks Corey parameters

6.2.2 Viscosity reduction with bacteria concentration

The viscosity of oil can be decreased drastically in the presence of bacteria. However, no conclusive experiment has been made to investigate how oil viscosity correlates with bacteria concentration Islam (1990). This thesis employs the correlation curve used in the paper being an analogy to solvent flood. We use an interpolation formula to derive the relation with some data points taken from the figure. Figure 6.8 displays the linear correlation curve between oil viscosity and bacteria concentration used in this thesis.

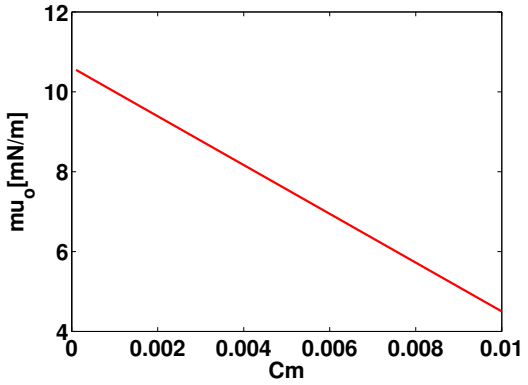

FIGURE 6.8: Viscosity correlation with bacteria concentration

In this simulation, an oil viscosity of 10 mPa.s was used together with the same reservoir conditions and parameters. Figure 6.10 compares recovery results of viscosity-reducing bacteria with that of water flooding after 45 days of simulation.

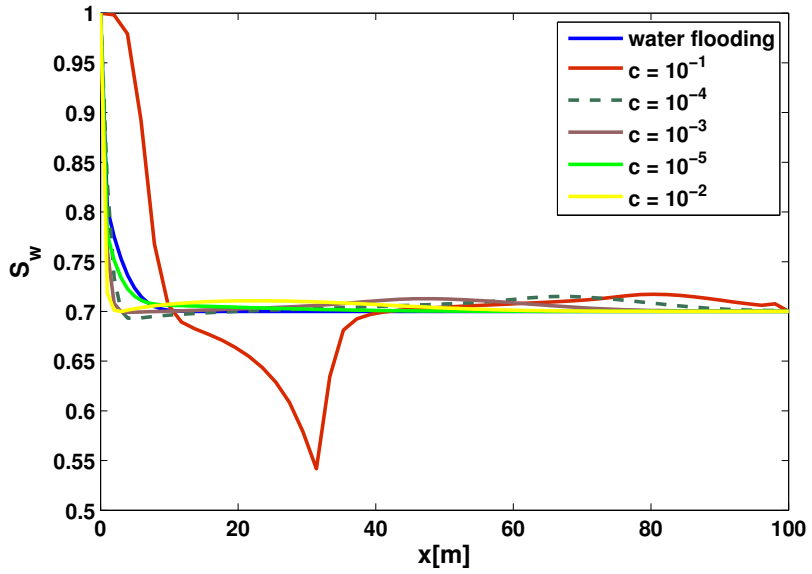

FIGURE 6.9: Saturation profile for van Genuchten parameter with focus on viscosity reduction

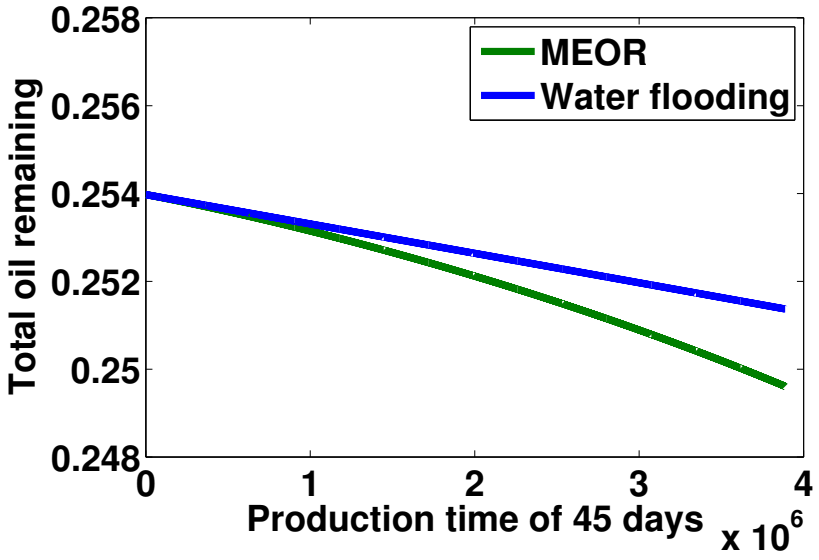

FIGURE 6.10: Fraction of oil remaining in the reservoire after 45 days with focus on viscosity reduction

The figure show that oil recovery declines in a similar way as water flooding. The only difference is the delay in the case of MEOR. We note that as the concentration of bacteria increases from ($C = 10^{-5} kg/m^3$) to ($C = 10^{-3} kg/m^3$), the recoveries are just similar to that of water flooding. The amount of oil recovered

with this range of bacteria solution are between 24.98% and 24.81%. Concentrations of ($C = 10^{-2}kg/m^3$) and ($10^{-1}kg/m^3$) gave quite a significant recovery of 24.69% and 24.48%. This indicates a sharp recovery as can be seen in the figure above. Although the fact still remains that bacteria have a positive effect on the residual oil in both mechanisms investigated, the percentage recovery from viscosity reduction bacteria are much less than bacteria generated surfactant flooding. Comparing concentration of ($C = 10^{-1}kg/m^3$) for both cases, bacteria generated surfactant flooding gave a final recovery of 20.79% as against 24.48% for the case of viscosity reduction bacteria. Figure 6.10 displays the fraction of oil left in the reservoir for a highly concentrated MEOR flooding as against water flooding with focus on viscosity reduction. Inter-facial tension reduction has always proven to be the best way to recover the residual oil. However, no candid conclusion can be made from this mechanism. Two factors of uncertainty are involved here. The first is that the nature of inter-facial tension reduction of oil viscosity are still not clear since this field lacks data. The second factor is that the presence of moderately viscous oil limits the benefit of oil viscosity reduction (Islam 1990).

6.3 Sensitivity analysis

We perform a sensitivity analysis using the van Genuchten's parameter n to see its effect on the sweep efficiency. With this simulation, we considered only the case of water flooding and a total production time of 100 days. Figure 6.11 and 6.12 displays the water profile curves and the fraction of oil remaining after 100 days. For $n = 2.5$ the total oil left is 15.6% whilst that of $n = 2$ gave 12.48%. With n as low as 1.5, a greater fraction of the oil has been recovered leaving just 6.28%. This reveals that as the parameter n decreases, the recovery increases. Similar arguments also hold for the Brooks Corey parameter λ in which as λ decreases, the recovery increases. The fact of the matter is that, these parameters are properties of the reservoir and cannot be altered. But a good knowledge of them will help to know which mechanism to employ for MEOR technology to be efficient.

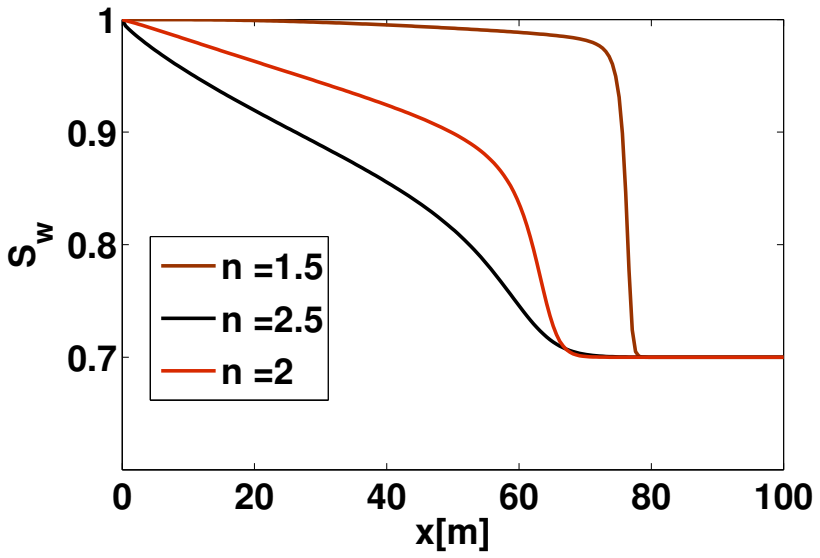

FIGURE 6.11: Water saturation profile for the sensitivity analysis of van Genuchten's parameter n

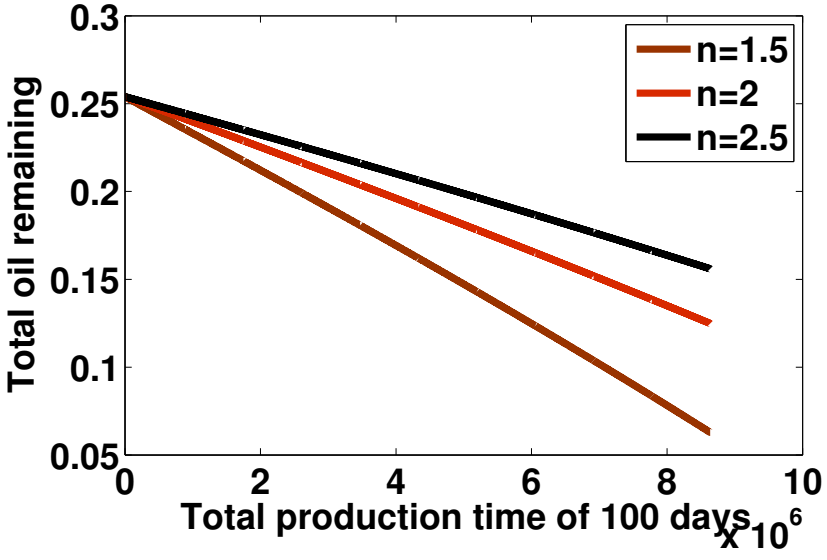

FIGURE 6.12: Fraction of oil remaining in the reservoir after 100 days with different van Genuchten's parameters

Reservoir model parameters and fluid properties

Parameter	Values
K	2 mD
ϕ	0.3
n	2
λ	2
L	100 m
T	45 days
P_e	2 MPa
ρ_w	1000 kg/m^3
ρ_o	800 kg/m^3
μ_w	0.869 x 10^{-3} $Pa\ s$
μ_o	9 x 10^{-4} $Pa\ s$
$\mu_o(base)$	10 x 10^{-3} $Pa\ s$
σ_{base}	29 mN/m
D	$1.92e-5$ m^2/s
S_{wi}	0.7
S_{or}	0.3
P_{wi}	2 MPa
P_e	2 MPa
C_{bi}	0 kg/m^3

TABLE 6.1: General parameters

Chapter 7

Summary and conclusion

This thesis presented a mathematical model for MEOR activities consisting of a two-phase flow and a transport equation. The model was discretized using the finite volume method and the IMPES approach. We validated our model by comparing it with the Couplex-Gas benchmark and with an analytical solution of which both proved the validity of the model. We assumed that the bacteria are affecting the inter-facial tension and the viscosity of the oil. Although several mechanisms exists for modeling MEOR activities, we investigated two of them.

Indeed our valid model has been able to showcase numerically that the activities of microbes does help in the recovery of the residual oil. This was seen in both mechanisms investigated. We first saw the case where inter-facial force reducing bacteria were introduced with various concentrations and their corresponding effect. The recovery curve in figure 6.5 of page 63 clearly shows that MEOR flooded surfactants had much oil recovered than conventional water flooding. We also saw in the second mechanism that bacteria affect the viscosity of the oil in a beneficial way. This was also demonstrated in figure 6.10, page 67 where viscosity reducing bacteria were seen to affect the residual oil. Comparatively, a reduction in the inter-facial force proves to be the best way to recover the residual oil as against viscosity reduction.

In this thesis, we have shown that the parameters of the relative permeability curves are very sensitive to the recovery. This was demonstrated in the case for the van Genuchten's parameter n where we discovered that the as n decreases, the

recovery increases. See figure 6.12, page 69. As reported by the paper Nielsen et al [28], it is indeed true that several parameters must be experimented so as to find a best fit with experimental data. Every reservoir has its own physio-chemical characteristics which ought to be well studied. This of course will provide a good clue on which species of bacteria to employ and which kind of mechanism to be used. If this is not factored, the notion of using MEOR, though will produce result but may not be optimum. In Nielsen et al (2003), they investigated a less efficient bacteria as against an efficient one in which the latter gave a recovery of 44% as against 9% by the former. Although comparatively, it is much lower, a 9% oil recovery is very significant.

It must be noted here that this thesis only provided a simple advection-diffusion equation which takes care of flow of bacteria in the water phase. The performance of MEOR would have been far better if growth of bacteria and substrate distribution has been factored. On the whole, MEOR is efficient and if well implemented can help recover the residual oil without causing much harm to the environment and will cut down high cost of oil production. Statoil has proven this fact and they are the only oil company so far in the world, using MEOR technology.

Outlook

- We hope to extend our advection-diffusion equation to a more general one which will address some challenges such as pore clogging, adhesion and adsorption etc facing MEOR transport.
- We look forward to consider other cases such as growth rates, substrate distribution coefficient where we can see the effects of bacteria leaving in both phases.
- To investigate all other possible mechanisms by which bacteria actions can be incorporated into the model in order to enhance the sweep efficiency.
- To come out with a new mechanism of modeling bacteria activities for the enhancement of the sweep efficiency.
- To consider higher dimensional modeling of MEOR activities.

Bibliography

[1] C. E., ZoBell, *"Bacterial Release of Oil from Oil-Bearing Materials (Part I)",* World Oil, vol.126, no. 13, 36-47, 1947.

[2] C. E.,ZoBell, *"Bacterial Release of Oil from Sedimentary Materials",* Oil & Gas 1., vol. 46, no.13, 62-65, 1974.

[3] C.E. ZoBell, *"The Effect of Solid Surfaces Upon Bacterial Activity"*, 1. Bact., vol. 46, 39-56, 1943.

[4] R. S. Bryant and T. E. Burchfield. *"Review of SPE Res. Eng.,* May, 151-154, 1989.

[5] Sino Australia Oil and Gas Limited. *An Introduction to Enhanced Oil Recovery Techniques.* Australia, 2013.

[6] Sen, R. *Biotechnology in petroleum recovery: The microbial EOR.* Progress in Energy and Combustion Science 34, 714-724, doi:10.1016/j.pecs.2008.05.001 (2008).

[7] Whitman WB, Coleman DC, Wiebe WJ. *"Prokaryotes: the unseen majority". Proceedings of the National Academy of Sciences of the United States of America*, 95 (12): 6578–83. 1998.

[8] C. M. Hogan. 2010. Bacteria. *Encyclopedia of Earth. eds. Sidney Draggan and C.J.Cleveland, National Council for Science and the Environment, Washington DC*

[9] T. F. Yen. *Microbial Enhanced Oil Recovery*: Principle and Practice , 1990.

[10] I. Aavatsmark. Bevarelsesmetoder for elliptiske differensialligninger. Lecture notes, University of Bergen, 2007.

[11] Jan M. Nordbotten and Michael A. Celia. *Geological Storage of CO_2. Modeling Approaches for Large-Scale Simulation.* Wiley, 2012.

[12] Z. Chen, G. Huan and Y. Ma. Computational Methods for Multiphase Flows in Porous Media. SIAM 2006.

[13] Florin A. Radu. Flow in Porous medium. Lecture notes, University of Bergen, 2013.

[14] J. H. Ferziger and M. Peric, *"Computational Methods for Fluid Dynamics"*."Finite Volume Methods" Springer, NY, 3rd edition, 2002.

[15] P. A. Markowich, C. Ringhofer, and C. Schmeiser, *Semiconductor Equations.* Wien-New York: Springer,1990.

[16] I. Danaila, P. Joly, S. M. Kaber, and M. Postel. *An Introduction to Scientific Computing, Twelve Computational Projects Solved with MATLAB.* Springer, 2007.

[17] C. F. Gerald and P. O. Wheatley. *Applied Numerical Analysis.* Pearson, 7th edition, 2004.

[18] D. Kincaid and W. Cheney. *Numerical Analysis: Mathematics of Scientific Computing.* Brooks/Cole, 3rd edition, 2002.

[19] F. A. Radu, A. Muntean, I. S. Pop, N. Suciu, and O. Kolditz. *A mixed finite element discretization scheme for a concrete carbonation model with concentration-dependent porosity.* Journal of Computational and Applied Mathematics, 246:74 85, 2013.

[20] F. A. Radu. *MAT260: Numerical Algorithms II - Lecture notes, University of Bergen, 2013.*

[21] I. Skjalaaen. Ph.D Thesis, *Mathematical Modeling of Microbial Induced Processes in Oil Reservoirs.* University of Bergen, 2010.

[22] J.F Schijven, S.M. Hassanizadeh. *Removal of Viruses by Soil Passage: Overview of Modeling, Processes, and Parameters.* Critical reviews in Environmental Science and Technology, volume 30(1): 49-127, 2000.

[23] M. V. Yates, S.R. Yates. *Modeling microbial fate in the subsurface environment.* CRC Crit. Rev. Environ. Control, volume 17(4):307-344, 1988.

[24] I. Aavatsmark 2007. *Multipoint flux approximation methods for quadrilateral grids*. Lecture notes, 9th International Forum on Reservoir Simulation, Abu Dhabi, 2007.

[25] J. W. Thomas. *Numerical Partial Differential Equations: finite Difference Methods.* springer, 1995.

[26] J. Monod. *The Growth of Bacterial Cultures.* Annual Review of Microbiology, v. 3, p. 371, 1949.

[27] B. Amaziane, M.Jurak and A. Z. Keko. *Modeling and Numerical Simulations of Immiscible Compressible Two-Phase Flow in Porous Media by the Concept of Global Pressure.*Pau (France), June 8-11, 2009.

[28] S. M. Nielsen, A. A. Shapiro, M. L. Michelsen and E. H. Stenby. *1D Simulation for Microbial Enhanced Oil Recovery with Metabolite Partitioning.* May 2010.

[29] M.R. Islam. *Mathematical Modeling of Microbial Enhanced Oil Recovery.*Alaska-Fairbanks, 1990.

[30] H. W. Bang and B. B. Caudle. *"Modelling of a Micellar/Polymer Process"*, Soc. Pet. Eng. 1., vol.24, 617-627, 1984.

[31] C. C. Emegwalu. *Enhanced oil recovery: Surfactant flooding as a possibility for the Norne E-Segment.*. Norwegian University of Science and Technology, 2009.

[32] F.A. Radu, J.M. Nordbotten, I.S. Pop and K. Kumar.*A robust linearization scheme for finite volume based discretizations for simulating of two-phase flow in porous media*, CASA report 14 - 25, 2014.